AECU-4356

MASTER

MASSACHUSETTS INSTITUTE OF TECHNOLOGY

Laboratory for Nuclear Science

TECHNICAL REPORT NO. 70

AUGUST 31, 1959

THE LATERAL DISTRIBUTION OF PENETRATING PARTICLES IN COSMIC RAY EXTENSIVE AIR SHOWERS

By

JAMES ARTHUR EARL

COSMIC RAY GROUP

B. B. ROSSI, Supervisor

DISCLAIMER

This report was prepared as an account of work sponsored by an agency of the United States Government. Neither the United States Government nor any agency Thereof, nor any of their employees, makes any warranty, express or implied, or assumes any legal liability or responsibility for the accuracy, completeness, or usefulness of any information, apparatus, product, or process disclosed, or represents that its use would not infringe privately owned rights. Reference herein to any specific commercial product, process, or service by trade name, trademark, manufacturer, or otherwise does not necessarily constitute or imply its endorsement, recommendation, or favoring by the United States Government or any agency thereof. The views and opinions of authors expressed herein do not necessarily state or reflect those of the United States Government or any agency thereof.

DISCLAIMER

Portions of this document may be illegible in electronic image products. Images are produced from the best available original document.

MASSACHUSETTS INSTITUTE OF TECHNOLOGY

Laboratory for Nuclear Science

TECHNICAL REPORT NO. 70

August 31, 1959

THE LATERAL DISTRIBUTION OF PENETRATING PARTICLES IN COSMIC RAY EXTENSIVE AIR SHOWERS

by

James Arthur Earl

Cosmic Ray Group

B. B. Rossi, Supervisor

Reproduction in whole or in part is permitted for any purpose by the U. S. Government. The data and the results which are presented in this report should not otherwise be published without prior consultation with the Laboratory for Nuclear Science.

The researches described in this technical report, which were completed prior to September 1957, have been supported in part by the National Science Foundation Grants G2055 and G3006 and in part by the U. S. Atomic Energy Commission and the Office of Naval Research under Contract Nonr-1841-(16).

TABLE OF CONTENTS

THE LATERAL DISTRIBUTION OF PENETRATING PARTICLES IN COSMIC RAY EXTENSIVE AIR SHOWERS

By

James A. Earl

Submitted to the Department of Physics on August 19, 1957, in partial fulfillment of the requirements for the degree of Doctor of Philosophy.

ABSTRACT

The penetrating component of extensive air showers detected by the MIT air shower experiment at Harvard, Massachusetts, has been observed with the aid of a large hodoscope shielded by 985 g/cm^2 of lead. The number of electrons, core location, and arrival direction of each shower were given by the air shower experiment. Mu-mesons associated with a shower could be identified by requiring the projected zenith angle as measured by the hodoscope to agree with the known arrival direction of the shower. An auxilliary detector consisting of a single heavily shielded tray of counters was operated 920 m from the center of the array. In showers with zenith angles less than 25° the density of mu-mesons is proportional to $r^{-1.0 \pm .2}$ for r between 20 and 150 m. (r is the distance from the shower core to the meson detector.) For r between 200 and 900 m the density is proportional to $r^{-2.2 \pm .1}$. The shape of the lateral distribution changes as the zenith angle of the showers is increased. The nature of this change is such that the mesons in inclined showers are more spread out than those in vertical showers. The effect of the magnetic field of the earth on the lateral distribution is small. The meson density near the core is proportional to $Ne^{.79 \pm .05}$ where Ne is the number of electrons in the shower. For showers with a constant observed number of electrons, the meson density near the core does not change with zenith angle. This fact implies that, in a shower of given primary energy, the

ABSTRACT -- continued

the density near the core decreases exponentially with depth with an absorption length of (253 ± 40) g/cm^2. The fraction of the mu-mesons with ranges greater than 540 g/cm^2 of lead which are absorbed in an additional 360 g/cm^2 of lead is (9. 9 ± 1. 5) %. This fraction is independent of distance to the core for r between 40 and 300 m.

I. INTRODUCTION

The study of the penetrating component of extensive air showers is a relatively direct way of investigating the cascade of high energy nuclear interactions which gives rise to a shower. In fact, most of the particles capable of discharging a Geiger-Muller counter under 20 cm or more of lead shielding are presumably either high energy nuclear active particles (π-mesons and nucleons) which are directly involved in the nuclear cascade or μ-mesons, which are the immediate decay products of charged π-mesons. Thus the penetrating particles are a much more sensitive indicator of the characteristics of high energy nuclear interactions than are the particles in the soft component which are related to π° mesons, produced in interactions only through many generations of electronic cascade multiplication. Even so, we cannot hope that the study of the penetrating component will yield anything more than some of the general features of high energy nuclear interactions. The presence of a nuclear cascade implies that the penetrating particles come from many interactions which are distributed over space and over a wide range of energies. Consequently, the behavior of the penetrating particles cannot be expected to reflect the detailed characteristics of any particular type of interactions.

Nevertheless, it is worth while to study large air showers because they are our only usable source of information on interactions with energies above 10^{15} ev. Interactions of up to 10^{14} - 10^{15} ev can be studied in emulsion stacks flown near the top of the atmosphere, but above 10^{15} ev the rate at which events are detected with stacks of reasonable size is so low that the method ceases to be practicable. In extensive air showers, on the other hand, the particles are spread with appreciable density over many thousands of square meters so that even events of 10^{17} ev are detected with a usable frequency.

Many studies of the penetrating component of air showers have been made. In most of these, detailed characteristics of each shower which triggered the apparatus were completely unknown; only the average characteristics of all the showers which triggered were known. The present investigation was undertaken in order to take advantage of the very detailed knowledge of individual showers which is obtained by the MIT air shower experiment at Harvard, Mass. This

experiment determines accurately the core location, the size (i.e., the number of electrons in the shower), and the arrival direction of each shower which triggers the array. This detailed knowledge permits the intensity of the penetrating component to be studied as a function of these quantities rather than as an integral over showers with a wide range of characteristics. This information is useful not only on its own merit but also as an aid to interpreting the results of less detailed experiments which, in some cases, are our only source of information about the penetrating component at altitudes other than sea level and at large depths underground.

Although most previous experiments on the penetrating component of air showers have been handicapped by incomplete knowledge of the size, core location, and zenith angle of the showers being detected, much significant information has been obtained. The value of the ratio of penetrating particles to electrons R_p has been measured at mountain altitudes (KHL 54) (SG 49) (GK 50) and at sea level (CB 48) (CG 49a) (TJE 48) in showers selected by threefold coincidences between unshielded trays of counters. In these experiments neither the core location nor the shower size was specified, so that the value of R_p represented an average over these variables. R_p has also been measured at mountain altitudes (CG 49b) and at sea level (FG 53) in showers selected by "core selectors." In these experiments the core location was specified by the requirement that the shower produce a highly multiple coincidence under thick lead shielding. Such a requirement does locate the core, but the rate at which cores of large showers trigger such a point detector is so low that the method is useless for studying showers having more than 10^6 electrons at sea level. Measurements of R_p extending to very large distances from the core have been made at mountain altitudes (ZGT 53) and at sea level (ELC 52) in showers whose cores were located by a close-spaced array of electron detectors. The present investigation differs from all of the above experiments in that our emphasis is on measuring the density of penetrating particles rather than the ratio R_p of penetrating particles to electrons and in that the knowledge of individual showers provided by the Harvard array is much more complete than that available in any of the above experiments. An experiment very similar to the present one has been performed at Harwell (PNA 57). However, in neither the Harwell experiment nor in any of the others were the zenith angles of individual showers measured. Since the Harvard experiment does give the arrival direction of each shower detected, the present experiment differs from all

the rest in that the penetrating component can be studied as a function of zenith angle.

An attempt has been made to take full advantage of the features of the Harvard array by covering as wide a range as possible of shower sizes and distances from the core. However, it is difficult to obtain much information about the immediate region of the core because, first, the rate at which the cores of the large showers detected by the air shower array strike near a detector is very low and, second, the density of penetrating particles in this region is so high that a penetrating particle detector with very good spatial resolution (a cloud chamber, for example) is needed to interpret correctly the complex events. For these reasons the emphasis in this work is on distances from the core of more than 20 m. This means that the penetrating particles with which we are dealing are essentially all μ-mesons because the nuclear active component is known to be confined within about 30 m of the core. Therefore, the penetrating particle detectors have been designed with large area so as to measure efficiently the small intensity of mesons far from the core and with provision for making unambiguous identification of μ-mesons. Thus the main objective of this experiment is to measure the lateral distribution of μ-mesons (i.e., the number of μ-mesons passing through a one-square-meter area as a function of distance from the shower core).

The lateral distribution is related to the properties of very high energy nuclear interactions. However, the analysis will be confined to a semi-phenomenological interpretation with the objective of saying as much as possible about the altitude and angular distribution of the μ's at production. This is being done instead of the alternative procedure of making a detailed comparison with the predictions of an assumed model of nuclear interactions, because the mathematical problem of finding the consequences of any particular model is prohibitively difficult and because the models which are available are not valid for the low energy interactions from which most of the μ-mesons arise.

II. DESCRIPTION OF THE EXPERIMENT

A. The Penetrating Particle Detectors

The MIT air shower experiment located at Harvard, Massachusetts (elevation 180 m) consists of eleven large scintillation counters distributed within a circle of 230 m radius. Figure 1 shows the locations of the penetrating particle detectors relative to the array of electron detectors. A large hodoscope (Detector 1) was operated in locations A (40 m from the center of the array) and B (300 m from the center). A heavily shielded tray of Geiger counters (Detector II) was operated at C (920 m from the center).

The two detectors are shown in Figure 2. Detector I was a shielded hodoscope consisting of two 48-inch by 48-inch trays of Geiger counters, one of which, A, was placed 17 inches above the other, B. Each tray was made up of 48 counters whose dimensions were 48 inches by 1 inch. The shielding consisted of 12 inches of lead plus 1 1/4 inches of iron between the trays and 18 inches of lead plus 1 1/4 inches of iron above the top tray. The hodoscope trays were also shielded by not less than 6 inches of lead on all sides and by 3 inches of lead plus one-half inch of iron between the bottom tray and the ground.

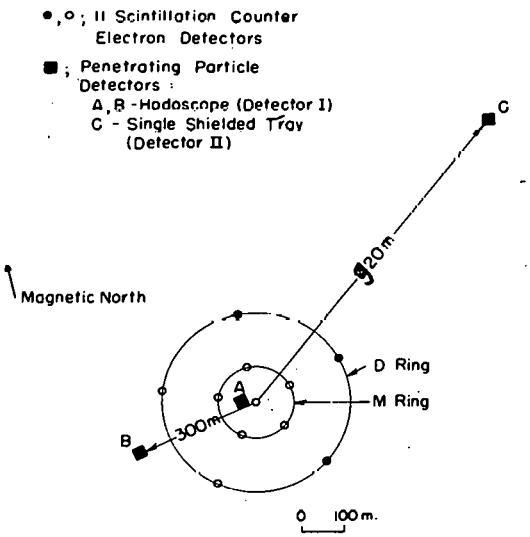

GEOMETRY OF EXPERIMENT

Figure 1

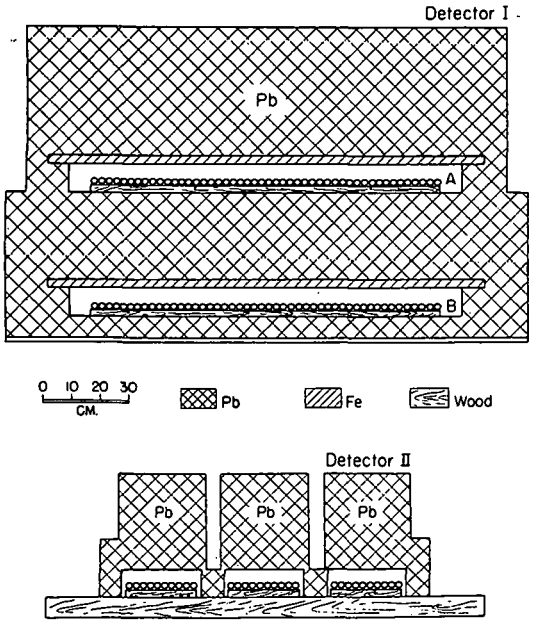

Figure 2

The total thickness of shielding above tray B was equivalent in stopping power to 985 g/cm^2 of lead. This thickness is certainly adequate shielding against the electronic component of showers, because Cocconi, Tongiorgi and Greisen (CG49a) have shown that only 250 g/cm^2 of lead is sufficient to reduce the effect of the electronic component to negligible proportions. More than this minimum thickness of lead was used in order to increase the average energy of the detected μ-mesons and to decrease the effect of low energy nuclear active particles.

An electronic circuit connected to each of the 96 tubes in the trays made a photographic record of all tubes that were discharged in coincidence with a master pulse coming from the air shower experiment. This arrangement made it possible to analyze complex events. For example, it was usually possible to distinguish penetrating showers produced in the lead from events in which several incident mesons penetrated the lead.

Detector II was a tray of 30 36-inch by 1 inch G-M counters shielded by 13 inches of lead. Whenever one or more counters were discharged a transistor circuit sent a pulse back to the central station where it was exhibited by an oscilloscope on the air shower experiment display panel. Detector II was used to study penetrating particles falling far from the core -- a region

where complex events associated with triggering air showers are so rare that elaborate hodoscoping is unnecessary.

Circuit details and methods of checking the operation of the apparatus are described in Appendix I. The apparatus was checked once a week and the counting rates of the two hodoscope trays and of the Detector II tray were continuously monitored on an Esterline Angus pen recorder. After an initial period of trouble shooting the equipment functioned very reliably except for occasional G-M counter failures..

B. Triggering Requirements for the Air Shower Array

Since the cores of most showers which satisfy the triggering requirement normally used for studying air showers with the Harvard array are clustered within about 90 m of the center of the array, it was necessary to use special requirements which resulted in distributions of cores which were more suitable for the study of the penetrating component. In no case, however, was the triggering influenced by signals from either penetrating particle detector. Therefore, the detected showers are in no way biased in favor of showers associated with penetrating particles.

The normal triggering requirement, which will be designated as (D+M+C), is that three or more electron detectors have pulses corresponding to a density of more than 10 p/m^2. The cores of showers which satisfy this requirement are clustered within the M ring of detectors (see Figure I). Another requirement, (D+M), which was satisfied by showers whose cores hit in the region between the M and D rings, was identical to the (D+M+C) requirement except that, in addition, a twofold coincidence of a greater than 10 p/m^2 pulse in any D-ring detector with a greater than 10 p/m^2 pulse in any other detector (including another in the D-ring) would satisfy the triggering requirement.

With Detector I in position A, the (D+M) requirement made it possible to study showers at distances from the core more than twice as great as those that were feasible with the normal triggering requirement. When Detector I was operated at position B, another special requirement (3D+M) was used in order to trigger efficiently on showers whose cores hit at the maximum usable distance from the detector. The (3D+M) requirement was identical to the (D+M) requirement except that only the greater than 10 p/m^2 pulses from the D detectors designated by ● in Figure I would satisfy the twofold coincidence requirement. A small amount of data was taken with various other special requirements which were designed to select especially small or especially large showers.

Table I gives the number of showers recorded with each combination of detector location and triggering requirement. With Detector II at position C the air shower array was operating essentially as a " core selector, " because the distance from C to the center of the array

TABLE I

Triggering Requirement	Detector Location	Range of distances from the core	Number of showers recorded
(D+M+C)	A	0 to 90 m	750
(D+M+C)	B	200 to 400 m	350
(D+M)	A	0 to 160 m	710
(3D+M)	B	200 to 400 m	900
(3D+M)	C	800 to 1000 m	1600
All other	---	----------	200

was considerably larger than the radius of the array. Although the triggering requirement used under these conditions was unimportant (3D+M) was chosen so that the same sample of completely analyzed showers used in conjunction with the data from Detector I at location B could be used with the data from Detector II. (See Section I-E).

For each shower detected with (D+M+C) triggering, the experiment can determine the arrival direction with an error of ±5°, the number of electrons in the shower with an error of 20% and the core location with an error of 10% of the distance from the core to the center of the array. With the special triggering requirements the information on showers striking far from the center is less precise to an unknown extent. However, this uncertainty is certainly much smaller than the uncertainty introduced by the necessity of grouping the showers in fairly broad ranges of these variables for the purpose of making the results statistically meaningful.

C. Interpretation of the Hodoscope Records

Our objective in interpreting the hodoscope record for each shower was to determine, with as little error as possible, the number of mesons which traversed both trays of the hodoscope. Ambiguity in the interpretation was much reduced by the fact that the projected zenith angle of any meson going through both trays could be compared with the projected zenith angle that would be expected from the known arrival direction of the shower. For a group of showers, a simple formula, which involves the geometry of the hodoscope and the zenith angle of the showers, relates the mean number of mesons which traverse both trays to the mean density of mesons.

Figure 3 shows some typical hodoscope records. There can be little doubt that records similar to (a) were caused by a number of parallel rays traversing the trays. This interpretation is almost completely unambiguous when the observed trajectories agree perfectly with the trajectories computed from the air shower arrival direction. For less clear-cut cases it is necessary to have objective criteria for interpreting "cluttered" records (such as b) and for throwing out impossible records (such as c). In setting up these criteria the main objective is to achieve a balance between throwing out too many true mesons and including too many false "mesons". The criteria used were set up with this in mind.

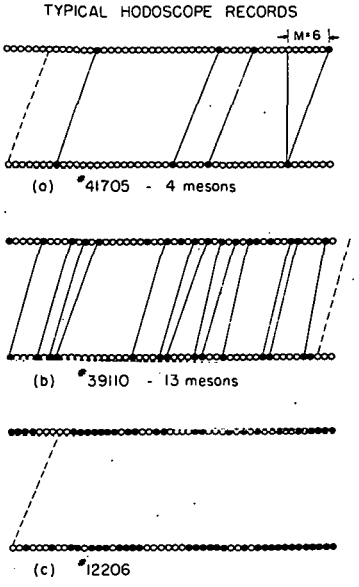

Dashed lines indicate projected zenith angle predicted from air shower arrival direction

Figure 3

In the work of analyzing the records it was convenient to specify the projected zenith angles by the horizontal displacement a particle would undergo in going from the top tray to the bottom tray. This displacement, M, which was measured to the nearest inch, is given by:

$$M = 17.8 \tan \theta_p \text{ inches} \qquad (1)$$

where θ_p is the projected zenith angle and 17.8 inches the distance between the trays. Figure 3a shows how M was measured in terms of the number of tubes between the discharged tube in the top tray and the tube directly above the discharged tube in the bottom tray.

The following criteria were used for identifying mesons in the hodoscope records:

1. (a) For each meson there must be at least one tube discharged in each tray.

   (b) If two adjacent tubes are discharged in each tray, the occurrence is counted as two mesons, provided M is less than 8 inches. If M is greater than 8 inches, the occurrence is counted as one meson.

   (c) All cases which involve two adjacent discharges in one tray and a single discharge in the other are counted as one meson.

2. In a record which involves a single meson, the observed displacement M_{obs} must agree with the displacement predicted from the arrival direction of the shower M_{pred} to within ± 4 inches.

3. In a record which involves two or more mesons, at least one meson must satisfy criterion 2 and the values of M_{obs} for all the mesons must be the same to within ±1 inch.

The reasons for Criterion 1 are obvious except for part b. This requirement helps to interpret correctly dense events in which there is a large probability that two separate mesons would produce adjacent discharges in both trays. The probability that a single meson would produce such an event is negligibly small for vertical mesons. The requirement that M be small ensures that mesons that can traverse two tubes in each tray because of their large inclination

are not counted double. Criterion 1 (c) is intended to include the fraction (about 7%) of the mesons which are accompanied by electrons as they emerge from the lead above one tray or the other.

Criterion 2 was intended to take into account the fact that the measurements of air shower arrival directions were not perfectly accurate. This criterion was made very loose because it was desirable to use some showers for which the experiment gave a very rough measurement of the arrival direction (D+M showers). Figure 4 is a histogram which shows the number of mesons accepted with various differences between the observed and predicted values of M. Figure 4 a refers to showers which satisfied the normal air shower triggering requirement and Figure 4 b refers to showers which satisfied only the twofold coincidence part of the (D+M) requirement. It can be seen from these histograms that the number of mesons for which the observed value of M differs by as much as 4 inches from the predicted is very small compared to the number with smaller deviations. We conclude from this that few true mesons were thrown out by Criterion 2. On the other hand, since we would expect false mesons to be evenly distributed among the intervals of the histogram, the number of false "mesons" in each interval can be no larger than the total number observed with deviations of 4 inches. If we assume that the number of false "mesons" is given by this upper limit, only 13% of the accepted mesons could be false.

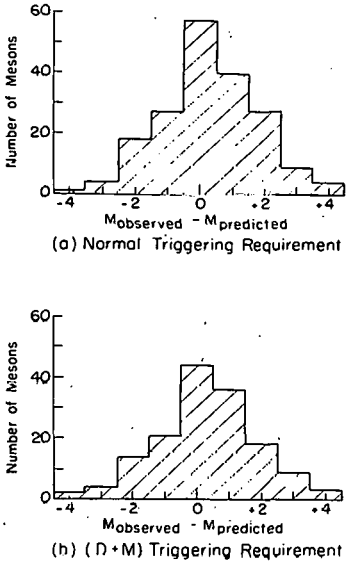

DISTRIBUTION OF DIFFERENCES BETWEEN OBSERVED AND PREDICTED ZENITH ANGLES

Figure 4

No correction has been made for the true mesons which were thrown out or for the false "mesons" which were included because the errors are small and tend to cancel each other.

Criterion 3 was intended as a further aid in correctly interpreting dense showers. In principle, one should always use the same requirement on the projected zenith angle irrespective of whether or not the mesons accepted are accompanied by others. In practice, however, application of Criterion 2 to all mesons would result in large errors for dense events because, for any discharge in either tray, there is a large probability that there would be another discharge in the other tray satisfying Criterion 2 whether of not the original discharge was actually associated with a true meson. By invoking a more rigid criterion for acceptance of mesons coming in groups, we remove this ambiguity at the expense of introducing a risk that the bias against widely scattered particles will depend on the density of the event. The importance of this effect depends on the degree to which the observed particles are actually scattered. Figure 5 is a histogram which shows the number of mesons with various deviations between the observed value of M and the mean value of M for all mesons in the event. An attempt was made to include in Figure 5 mesons which were rejected under Criterion 3. Every event used had two or more mesons. It is clear from Figure 5 that, on the average, associated mesons do tend to be very nearly parallel.

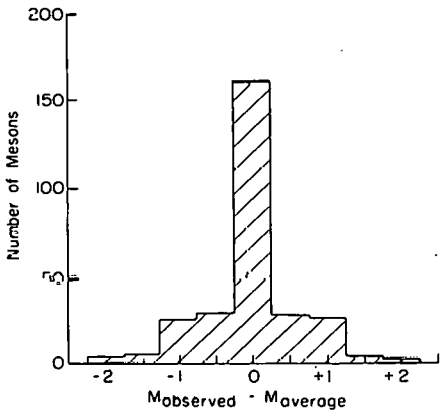

DISTRIBUTION OF PROJECTED ZENITH ANGLES IN EVENTS WHICH HAVE MORE THAN ONE MESON

Figure 5

On the strenght of this fact, we feel that Criterion 3 introduces little bias.

The application of these criteria to artificial events which were generated with the aid of a table of random numbers, showed no obvious systematic errors. In general, the process of

interpretation was much simpler than the preceding discussion would indicate because most of the records were so "clean" that it was easy to interpret them. The event shown in Figure 3a is a very typical event. Only when shower cores hit near the detector were the hodoscope records so complex that their interpretation was ambiguous. In the following, all data appreciably affected by ambiguous events have been thrown out. In practice this meant that the measurements within a certain distance of the core (this distance depended on the shower size) have been thrown out. It will be shown later that the densities deduced from interpretation of the hodoscope records agree well with densities deduced from the number of tubes discharged in the bottom tray.

The following formula, which is derived in Appendix II, was used to relate the density ρ to the number of mesons traversing both trays N_μ:

$$\rho = \frac{N_\mu}{A \cos\theta \left\{1 - \frac{4}{\pi} \frac{d}{\ell} \tan\theta\right\}} \qquad \text{II} \quad (2)$$

where ρ is the density, A is the area of the trays, θ is the zenith angle of the showers, d is the distance between the trays, and ℓ is the length of the square trays. The factor $4/\pi$ comes from an averaging integral over the azimuthal angles.

D. Analysis of the Signals from Detector II

The pulses from Detector II were displayed on an oscilloscope with a 50 μsec sweep. With this method of display it was possible to discriminate against accidental pulses which came at times incompatible with the time of arrival of the showers. The effective resolving time for accidental coincidences could have been made as short as the rise time of the pulses, which was about 1 μsec, but, in practice, a somewhat longer resolving time was found to be satisfactory.

Figure 6 shows the distribution of measured delay times for all pulses from Detector II, which were observed on sweeps triggered by showers. The data for this plot includes some taken with the Detector II tray unshielded. It is clear that there is a marked clustering of delays around a value corresponding to a deflection of 5 mm, which is approximately what would be expected from a consideration of the length of the Detector II cable and the various delays involved in the triggering of the air shower experiment. All pulses with deflections between 3 and 7 mm were counted as "true" associated pulses. This range was made wide enough so that pulses from highly inclined showers would not be counted as false.

Table II gives pertinent information on the data taken with Detector II.

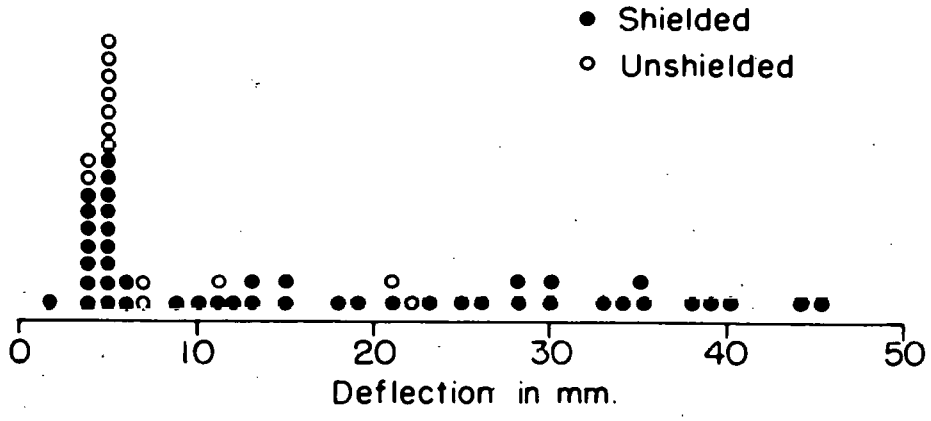

DISTRIBUTION OF DELAY TIMES OF PULSES FROM DETECTOR II.

Figure 6

TABLE II

	Number of true pulses 3-7 mm	Number of "false" pulses 10-40 mm	Total number of sweeps	Expected number of "false" in the 3-7 mm interval
Shielded	18	23	1600	3
Unshielded	11	3	534	.3

From the last column in this table it can be seen that the accidental pulses that were included among the "true" pulses contribute a small error. In the following analysis this error has been subtracted out for each group of showers considered.

E. Analysis of the Data

All pertinent data for each shower were punched onto a standard IBM card. Table III is a key to the information recorded on each card.

The most significant items recorded were the shower size N_e (i.e., the total number of electrons in the shower), the zenith angle θ, the distance r from the core to the meson detector and number of mesons going through both trays N_μ. The last of these was determined from the hodoscope records in accordance with the rules set forth previously, while the rest were obtained as results of calculations performed by the Whirlwind computer on data obtained from the electron detectors.

Once these data had been punched on cards the showers were sorted into groups according to their size, zenith angle, and distance from the meson detector. The range included in each of these groups is shown in Table IV, together with the code numbers identifying each grouping. The size ranges are logarithmic intervals corresponding to a factor of about 3. The zenith angle intervals were chosen so that the mean thickness of atmosphere traversed would increase by 100 g/cm ^{2} in going from one group to the next. The core distance ranges are logarithmic intervals such that the mean distance for each group is greater than that for the preceding group by a factor of about 1.6.

TABLE III

IBM Card Format

Column Number	
1-4	Serial number
6-10	Air shower experiment sequence number
12-15	Time of arrival of air shower
17, 18	Shower size N_e
19	Exponent of power of 10 multiplying N_e

TABLE III - continued

Column Number	
21-23	X co-ordinate of core
25-27	Y co-ordinate of core
29, 30	Zenith angle θ
32-34	Azimuthal angle ϕ (measured from geographic north)
36-38	Distance from core to meson detector
40-43	Measured electron density
45-48	Computed electron density
50, 51	Number of mesons traversing both trays N_μ
53-57	Record of tubes discharged in Tray B
58-62	Record of tubes discharged in Tray A
63	Code number specifying azimuth of core with respect to meson detector.
64	Zenith angle interval θ_N
65	Shower size range N_N
66-67	Distance interval r_N
77, 78	Number of tubes discharged in Tray B N_B
79, 80	Number of tubes discharged in Tray A N_A

TABLE IV

Size, Zenith Angle and Core Distance Intervals

Code Number N_N	Column 65 Size Range
1	$1\text{-}3 \times 10^5$ electrons
2	$3\text{-}10 \times 10^5$
3	$1\text{-}3 \times 10^6$

TABLE IV - continued

Code Number N_N	Column 65 Size Range
4	$3\text{-}10 \times 10^6$
5	$1\text{-}3 \times 10^7$
6	$3\text{-}10 \times 10^7$
7	$> 10^8$

Code Number θ_N	Column 64 Zenith Angle Interval
1	0-25°
2	25-33°
3	33-40°
4	40-45°
5	> 45°

Code Number r_N	Columns 66 and 67 Core Distance Interval
1	0-20 m
2	20-30 m
3	30-50 m
4	50-80 m
5	80-130 m
6	130-210 m
7	210-340 m
8	340-430 m

An IBM accounting machine (Type 406) was used to tabulate significant data for each shower and to add up sums needed for the preparation of lateral distributions and for the computation of the mean size, zenith angle, and distance of the showers in each group.

Most showers recorded with Detector I at 300 m from the center (Position B) and with Detector II give no indication whatsoever in the meson detector. Since the labor of preparing cards for analysis is considerable, it would be very desirable to process only those showers which did give an indication in the meson detector. This has been done for a large group of showers. The average characteristics of the unanalyzed showers were assumed to be identical to those of a sample of 242 showers obtained under identical conditions but fully analyzed. In this way it was possible, in the case of Detector I at position B, to use the data on mesons from 663 showers while processing only 150 of them and, in the case of Detector II, to use the data on 1600 showers while processing only 18. Since this procedure is equivalent to analyzing all the showers (except for a slight increase in the statistical errors), no bias is introduced provided that the triggering requirements do stay constant. Since the counting rate of the air shower experiment depends sensitively on these requirements and since no variation of this rate was observed during the period in question, the data are probably not affected much by variation in triggering requirements.

III. EXPERIMENTAL RESULTS

The most significant results have to do with the main objective of the experiment, which was to measure the lateral distribution of mumesons in showers having a wide range of sizes and zenith angles. Results have also been obtained on the absorption of the mesons in lead, on the effects of the magnetic field of the earth on the lateral distribution of mesons and on the ratio of the meson density to the total density of charged particles.

The data on the meson component of showers is useful in studying the development of showers in the atmosphere. The development starts when the high energy primary cosmic ray interacts with an air nucleus in the upper atmosphere and produces a number of high energy secondary particles. The number of particles in the shower increases as the chain reaction initiated by these secondary particles developes, but, at a certain atmospheric depth, a maximum is reached because the average energy of the particles becomes so low that the mean number of particles produced in each new interaction is less than one. Below the maximum, the number of particles decreases with increasing depth as the energy in the shower becomes dissipated. The showers in the size range we have studied are well past their maximum development at sea level. Since it is likely that the shower development depends only on the thickness of atmosphere traversed, a comparison of the properties of inclined showers with those of vertical showers can yield information on the development of showers because the inclined showers have gone through a greater thickness of air than have the vertical showers.

All the results which will be presented refer to averages over large numbers of showers with similar characteristics. For example, each point on a lateral distribution curve is the average density for a group of showers whose distances from the core lie in a certain interval. This point is plotted at the average distance from the core for all the showers in the group. It can be shown that this use of the average distance approximately compensates for variations with distance of the triggering probability of the showers. The use of average zenith angles and shower sizes has eliminated other errors of similar nature.

Tables presented in Appendix III summarize the data on which the results are based.

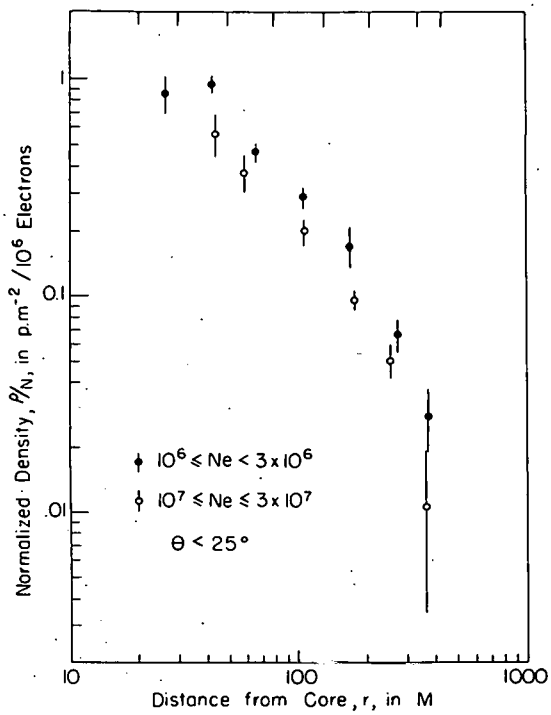

LATERAL DISTRIBUTIONS FOR TWO GROUPS OF SHOWERS WITH DIFFERENT MEAN SIZES

Figure 7

A. Dependence of the Shape of the Lateral Distribution on Shower Size and on Zenith Angle

Figure 7 shows the lateral distributions of mesons in two groups of near vertical showers whose mean sizes differ by a factor of 8. The abscissa of each point is the mean distance from the core to the meson detector r for the showers falling in each of the radial intervals indicated near the top of the figure. The ordinate is the mean meson density normalized with respect to the shower size ρ/N (i.e., the meson density ρ divided by the mean number of particles N in the showers of the group). The purpose of normalizing the densities is to correct approximately for a small systematic variation of mean shower size with distance from the meson detector. This variation, which arises because the triggering probability for showers of a given size strongly depends on the distance from the core to the center of the array, could distort the shape of the lateral distribution if it were not taken into account.

We see from Figure 7 that the curve for a mean size of 2×10^6 lies above the curve for 1.5×10^7 by a factor of about 1.3, but that, within the statistical accuracy of the data, there is

no detectable difference in the shapes of the two curves. Although the fact that the two curves do not quite coincide indicates that the density of mesons does not increase in exact proportion to the shower size, it is apparent that the normalized density is approximately independent of shower size since it changes by only a factor of 1.3 for a factor of 8 change in shower size.

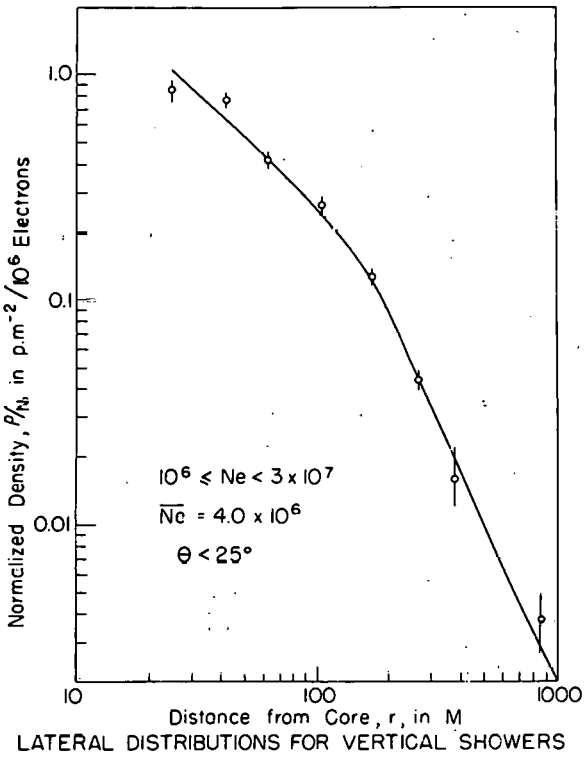

LATERAL DISTRIBUTIONS FOR VERTICAL SHOWERS

Figure 8

Since neither the normalized density nor the shape of the lateral distribution show a strong dependence on shower size, it is justifiable to combine the normalized densities from showers in a wide range of sizes in order to increase the statistical accuracy of the determination of the shape of the lateral distribution. Figure 8 shows the mean normalized density as a function of distance to the core (over the range 20 to 850 m) for showers with sizes in the range 10^6 to 3×10^7 electrons and zenith angles less than 25°. The co-ordinates of this plot are defincd in the same way as those of Figure 7. From Figure 8 we see that there is a change in the form of the lateral distribution at approximately 150 m from the shower core. Indeed, for r between 20 and 100 m, the normalized density is proportional to $r^{-1 \pm .2}$ while for r between 150 and 850 m the

density is proportional to $r^{-2.2 \pm .1}$.

The total number of mesons in a shower is given by:

$$N_\mu = \int_0^\infty 2\pi r dr \rho(r) \qquad \text{III} \quad (1)$$

where $\rho(r)$ is the meson density at a distance r from the core. Since ρ has been measured only at distances less than 900 m from the core, it is not possible to evaluate this integral from the experimental data without making an extrapolation to take into account mesons falling more than 900 m from the core. From the experimental results presented in Figure 8 we obtain:

$$N_\mu \ (r < 900 \text{ m}) = (2.2 \pm .4) \times 10^5 \text{ mesons}$$

for the total number of mesons falling within 900 m of the core of showers of mean size 4.0×10^6 electrons. (This result includes a small contribution from mesons falling within 20 m of the core which was obtained by extrapolating the density distribution to r = 0 according to $\rho \alpha r^{-1}$.) Assuming that $\rho = kr^{-2.2}$ for r greater than 900 m, we obtain:

$$N_\mu \ (r > 900 \text{ m}) = (3.6 \pm 2.0) \times 10^5 \text{ mesons}$$

for the number of mesons falling further than 900 m from the core. Since it is very unlikely that the meson density decreases less rapidly than in proportion to $r^{-2.2}$ at any point beyond 900 m this estimate is probably an upper limit on the number falling beyond 900 m. For the sum of these two estimates we obtain:

$$N_\mu = (5.7 \pm 2.2) \times 10^5 \text{ mesons}$$

for the total number of mesons in showers of mean size 4.0×10^6 electrons and zenith angle less than 25°. This implies that the ratio of mesons to all charged particles in these showers is $(14 \pm 5)\%$. Since our estimate of the number of mesons falling more than 900 m from the core was based on little more than speculation, this estimate of the total number of particles does not

have very great significance as an experimental result (although it probably can be considered as an upper limit on the total number). On the other hand, we have considerable confidence in our determination of the number of mesons within 900 m of the core. The ratio of this number to the total number of particles in the shower is (5.5 ± 1.0) %.

The root-mean-square radius r* for a lateral distribution is given by:

$$r^{*2} = \frac{1}{N_\mu} \int_0^\infty 2\pi r^3 dr \rho(r) \qquad \text{III} \quad (2)$$

where N_μ is defined by Equation III(1). It is not possible to do more than set a lower limit on r* from the experimental data, because the extrapolation used in estimating N_μ leads to a divergent integral in the definition of r^{*2}. From the results presented in Figure 8 we obtain:

$$r^{*2} > 330 \text{ m}$$

as a lower limit on the root-mean-square radius of mesons in showers of mean size 4.0×10^6 electrons and zenith angle less than 25°. The fact that the integrand of Equation III (2) is still increasing with r at the limits of the measurements indicates that the true r* (if it exists) is probably considerably larger than this lower limit.

Figure 9 shows the observed lateral distributions for showers with zenith angles greater than 25°. The showers have been divided into two groups having mean zenith angles of 28° and 36°. The solid line is the comparable curve for vertical showers (Figure 8). In Figure 9, approximate corrections for the effects of variations with zenith angle of the mean measured size of detected showers have been made. Consequently, the normalized densities are proportional to the densities that would be obtained for showers with a constant number of electrons but varying zenith angles.

A comparison between the curves for different angles in Figure 9 shows that the meson density near the core increases by a factor of 1.3 as the zenith angle is varied from 0° to 40°. It is apparent that the normalized densities at large distances from the core (200 - 900 m) increase

by a larger factor when the zenith angle is increased than do the densities near the core (20 to 150 m). This implies that the mesons in steeply inclined showers are more spread out than are those in vertical showers.

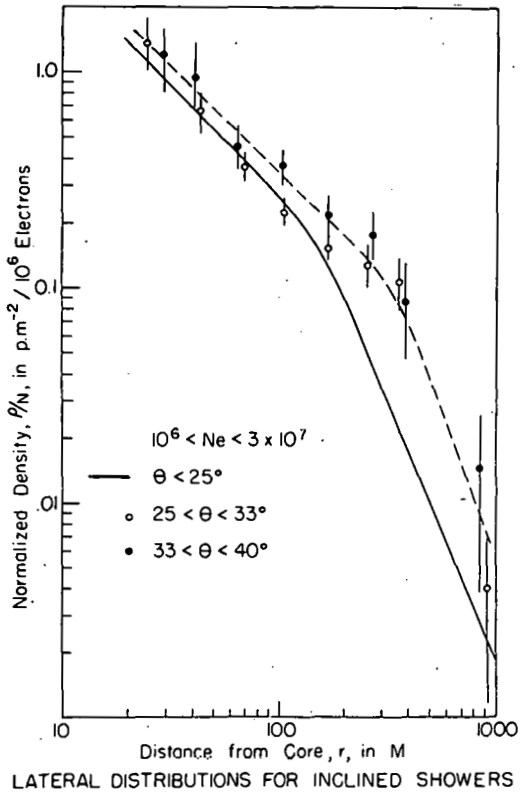

LATERAL DISTRIBUTIONS FOR INCLINED SHOWERS

Figure 9

The statistical accuracy of the density measurements plotted in Figure 9 is so poor that the procedure previously used to determine the number of mesons in vertical showers yields only a rough estimate of the number of mesons in inclined showers. The combined data for the two zenith angle ranges gives:

$$N_\mu \ (r < 900 \text{ m}) \quad = \quad (5 \pm 1) \times 10^5 \text{ mesons}$$

for the number of mesons falling within 900 m of the core of showers with zenith angles in the range 25° to 40° (mean angle 30°) and with a mean size of 4×10^6 electrons. No attempt has been made to extrapolate the lateral distribution beyond 900 m because the data for r less than

900 m is not accurate enough to justify such an extrapolation. This value of N_μ is a factor of 2.3 greater than the corresponding number of mesons in vertical showers. This large ratio contrasts with the small value which was obtained for the ratio of densities near the core. The difference lies in the dependence of the shape of the lateral distribution on zenith angle.

B. Dependence of the Density Near the Core on Shower Size

For the purpose of studying the density near the core it is useful to define a quantity K such that:

$$\rho(r) = \frac{K}{r} \qquad \text{III} \quad (3)$$

where ρ is measured in particles per m^2 and r in m so that K has the dimensions of m^{-1}. Since it is apparent from Figures 7 and 9 that the density near the core is approximately proportional to r^{-1} independent of size and zenith angle, K is essentially a normalizing constant which is independent of distance from the core over the region $20 \text{ m} < r < 150 \text{ m}$.

In connection with Figure 7, we have observed that the meson density near the core varies with shower size but is not exactly proportional to N_e. We will now express this fact more precisely by determining how K depends on N_e over a wide range of shower sizes. Density measurements based on interpretation of hodoscope records are not ideal for this purpose because of possible sources of error in especially large and especially small showers. In small showers, the density may be underestimated because the arrival directions are so poorly determined by the air shower array that true mesons may be thrown out under acceptance Criterion 2 (Section I C). In large showers the meson density is so high that there is an appreciable probability that two mesons are so close together that they may be counted as one under Criterion 1(b). Both of these sources of error can be eliminated by using the total number of discharges in the bottom tray as a measure of density. The error in small showers is eliminated because the number of discharges is obviously independent of measurements of the shower direction. The error in large showers is automatically eliminated by the use of the correct method of relating the number of discharges to the meson density.

The mean number of discharges in an event with density ρ is:

$$\bar{n} = 48 \left(1 - e^{-\rho A}\right) \qquad \text{III} \quad (4)$$

where A is the area of each of the 48 tubes in the tray. Since the density ρ is confined to a narrow range of values by the requirement that all showers in a group have roughly the same size and distance from the core, it is safe to infer the mean density ρ directly from this expression without special consideration of the a priori distibution of ρ. The fact that ρA in Equation III (4) is never more than .3 is a further argument for the validity of this procedure. By manipulating Equation III (4) we obtain the approximate relation:

$$\rho = \frac{1}{A} \frac{\bar{n}}{48} \left(1 + \frac{1}{2} \times \frac{\bar{n}}{48} \right) \qquad \text{III} \quad (5)$$

where $\bar{n}$ is the mean number of discharges in the showers under consideration and A is the area of each tube. Although this expression is not exact it gives ρ accurately enough for our purposes since the error introduced by the approximation is less than 2% as long as ρA is less than .3. The term $1/2 \frac{\bar{n}}{48}$ inside the brackets in Equation III (5) can be interpreted as the correction for high densities which is necessary for the correct analysis of data from large showers.

For the determination of K, only the data for showers with r between 30 and 130 m were used. This restriction is necessary because, for r less than 30 m, an appreciable fraction of the discharges in the bottom tray was caused by the products of nuclear interactions occurring in the lead -- not by μ mesons already present in the shower -- and because, for r greater than 130 m, ρ is no longer proportional to r^{-1}. The actual value of K used was computed from the following formula:

$$\bar{K} = \sum_i (\rho_i r_i) n_i / \sum_i n_i \qquad \text{III} \quad (6)$$

where ρ_i is the mean density computed for radial group i from Equation III (5), r_i is the mean radius and n_i is the total number of discharges in the bottom tray for all the showers in the group.

Figure 10 shows K computed as outlined above as a function of shower size N_e. The value of K based on densities determined from interpretation of hodoscope records for $\bar{N}_e = 1.9 \times 10^6$ electrons has been included as an open circle in order to show that the two methods of measuring densities give comparable results under circumstances where the sources of error mentioned

earlier are not important. The small remaining discrepancy can be attributed to double discharges caused by knock-on electrons which accompany the mesons as they emerge from the lead. A correction for this effect could be estimated from the known values of the probability that a meson unassociated with air showers is accompanied by an electron with sufficient energy to penetrate the counter walls. (BWW49a) However, since the energy spectrum of the mesons in air showers may be different from that of unassociated mesons, it was felt that it would be better to normalize the final results to the value of K determined with the hodoscope for $\overline{N}_e = 1.9 \times 10^6$ electrons.

This normalization gives a result which is practically identical to the result that would have been obtained if the correction based on measurements on unassociated mesons had been applied. A small additional correction has been applied to the values of K for N_e less than 10^6 electrons in order to take into account the fact that some of the data for these points were taken with 24 inches of lead instead of 30 inches above the bottom tray. This correction was based on the values of K with and without the extra lead for N_e between 10^6 and 3×10^6 electrons. The ratio of these values was $1.1 \pm .2$. All the data used in the determination of K for values of N_e greater than 10^6 were taken with the full 30-inch layer of lead.

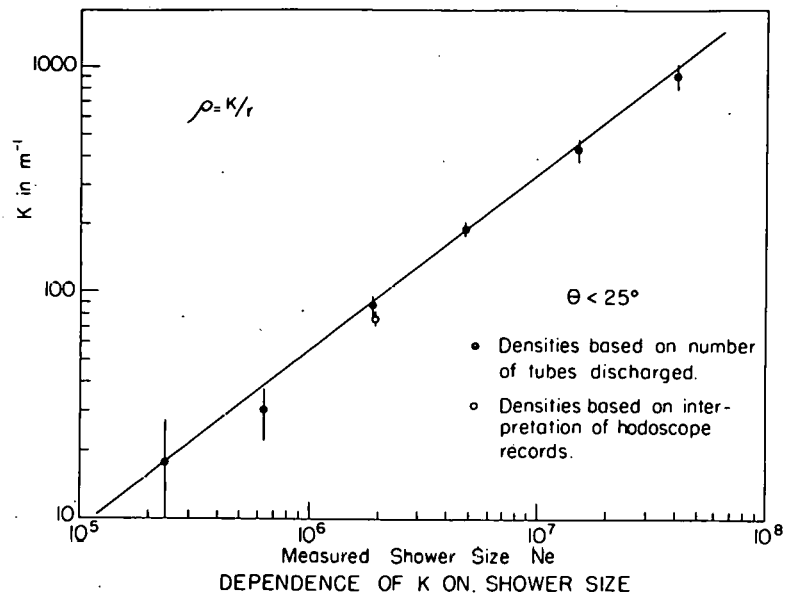

DEPENDENCE OF K ON SHOWER SIZE

Figure 10

It is apparent from Figure 10 that the dependence of K on N_e is well represented by a power law. Normalizing the values of K based on the number of discharges in the bottom tray to

the value of K obtained from interpretation of hodoscope records at $\bar{N}_e = 1.9 \times 10^6$ we obtain:

$$K = (46.5 \pm 2)\ (N_e/10^6)^{\ .79 \pm .05}\ m^{-1} \qquad \text{III (7)}$$

for N_e in the range 2×10^5 to 10^8 electrons and for mesons observed in the range 30 to 130 m from the core.

We have already seen that there is some evidence that the shape of the meson lateral distribution is independent of shower size. If this result were strictly true, then K would be a measure not only of the density near the core but also of the total number of mesons in the shower. By combining our result on the number of mesons within 900 m of the core of showers of mean size 4×10^6 electrons with the measured dependence of K on N_e, we obtain:

$$N_\mu (r < 900\ m) = (.73 \pm .1) \times 10^5 \times \left(\frac{N_e}{10^6} \right)^{.79 \pm .05} \qquad \text{III (8)}$$

for vertical showers under the assumption that the lateral distribution is independent of N_e.

Calculations of the nuclear cascade based on the Landau model of high energy nuclear interactions have been made by Olbert and Stora (OS 57). These calculations yield the result that

$$N_e \ \alpha \ E_o^{\ 1.16}$$

where E_o is the energy of the primary cosmic ray and N_e is the number of particles at sea level. If we accept this result, we obtain

$$K \ \alpha \ E_o^{\ .92 \pm .06} \qquad \text{III (9)}$$

C. Dependence of the Meson Density Near the Core on Zenith Angle

We have already seen from Figure 9 that the normalized meson density near the core is almost independent of zenith angle for showers with a fixed number of electrons. In Figure 11 we present more results bearing on this question. The abscissa is the atmospheric depth x measured in the average direction of the shower axes. For a group of showers with average zenith angle $\bar{\theta}$, x is related to the vertical depth x_0 by $x = x_0/\cos\bar{\theta}$. The ordinates of the solid points are measured values of K computed with the aid of Equations III (3) and III (6) using densities inferred from interpretation of hodoscope pictures. We see that K is nearly independent of x for x less than 1300 g/cm^2 and that the curves for the various size ranges are parallel within experimental errors.

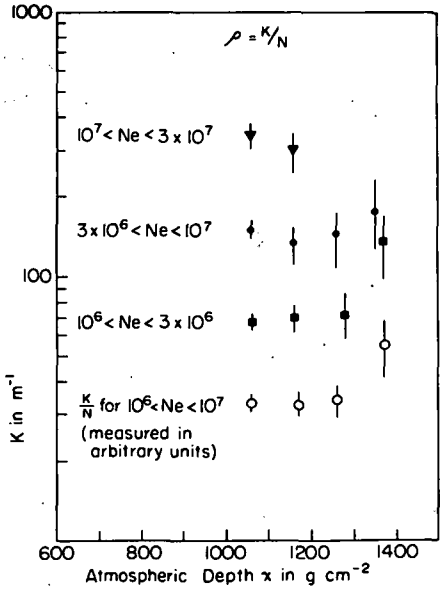

DEPENDENCE OF K ON DEPTH FOR CONSTANT MEASURED SIZE

Figure 11

In order to obtain a more exact idea of the form of the relation between K and x, we have plotted as open circles on Figure 11 the values of K/N obtained by combining the data from all showers with size between 10^6 and 10^7 electrons. If we assume that K varies exponentially with depth, i. e.,

$$K = \text{constant} \quad e^{-\frac{x - x_0}{L}}$$

where L is a constant, we obtain from these values of K/N

$$\frac{1}{L} = + (1 \pm 5) \times 10^{-4}\ g^{-1}\ cm^2$$

provided the point at $x = 1370\ g/cm^2$ is ignored. Since this result implies that K changes very slowly (if at all), with increasing x, we must conclude that, for depths less than $1300\ g/cm^2$, the meson density near the core is essentially independent of depth for showers with constant observed size.

This conclusion would be essentially unaltered even if there were systematic errors (due to misinterpretation of the hodoscope records) in the correction factor $f(\theta)$ by which the observed number of mesons at a zenith angle θ must be multiplied in order to get the density. (See Equation II (2).) Even if the variation of $f(\theta)$ were ignored completely, the apparent value of 1/L which would be obtained if K were truly independent of x would be only

$$\frac{1}{L_{APP}} = - \frac{1}{550\ g/cm^2}$$

Since the uncertainty due to systematic errors in the evaluation of $f(\theta)$ is probably less than the correction itself, this value of 1/L represents an upper limit on systematic errors from this source. A re-examination of some of the hodoscope records for showers with large zenith angles led to the conclusion that, even at large angles, the interpretation of the pictures was usually unambiguous, so it is unlikely that there is actually much error due to misinterpretation of the hodoscope records.

The points at $1370\ g/cm^2$ appear to lie significantly higher than the points at smaller depths. This could be due to a statistical fluctuation, a systematic error, or a real effect. Since the chance for systematic errors is largest at large angles and since it is possible that fluctuations in shower development could lead to a real effect of this type, this point was neglected in the determination of 1/L.

While it is significant that K is independent of x for a fixed observed size, what is really

wanted is the dependence of K on x for a fixed primary energy. For this purpose, we introduce the equivalent vertical size of a shower defined by:

$$N(x) = N(x_o)\, e^{\frac{-(x-x_o)}{\lambda}} \qquad \text{III (10)}$$

where $N(x)$ is the size of the shower observed at depth x, $N(x_o)$ is the equivalent vertical size (i.e., the size that would be observed at depth x_o if the shower had come in vertically) and λ is a constant absorption legth. There is considerable evidence from the variation of the rate of detection of air showers with altitude, with pressure and with zenith angle (CGW 57) (GK 56) that Equation III (10) is valid near sea level for showers of the size we are concerned with and that the value of λ is near 200 g cm^{-2}.

If Equation III (10) is valid and if fluctuations in shower development are neglected, then a given equivalent vertical size corresponds to a unique primary energy. Thus our objective is to find the dependence of K on x for a fixed equivalent vertical size. We shall use the value $\lambda =$ 200 g/cm^2. (The uncertainty in this value is about 30 g/cm^2 (CGW 57).)

We shall assume that the values of K for showers observed at depth x with N electrons can be represented by a law of the form:

$$K(x,N) = F(x)\, N^{\beta} \qquad \text{III (11)}$$

where, according to our measurements, $F(x)$ is essentially a constant and $\beta = .79$. Although the data taken at large zenith angles are not complete enough to verify this assumption with any degree of certainty, the fact that the curves in Figure 11 for showers with various sizes are nearly parallel indicates that the experimental results are not in violent disagreement with this assumption.

If we now substitute in Equation III (11) the value of N from Equation III (10) we get:

$$K(x, N) = F(x)\, e^{-\frac{(x-x_o)}{(\lambda/\beta)}} \quad [N(x_o)]^{\beta} \qquad \text{III (12)}$$

which is an expression giving K as a function of equivalent vertical size and of x. If we express F(x) as an exponential function:

$$F(x) = Ae^{\frac{x-x_0}{L}} \qquad \text{III (13)}$$

we obtain from Equation III (12)

$$K(x, N(x_0)) = Ae^{-\left[\frac{1}{(\lambda/\beta)} - \frac{1}{L}\right](x-x_0)} \times [N(x_0)]^{\beta} \qquad \text{III (14)}$$

This result implies that, for a constant equivalent vertical size, K varies exponentially with depth with the absorption length

$$\Lambda = \lambda/\beta \quad \frac{1}{1 - \lambda/\beta L} \qquad \text{III (15)}$$

Using our measured values of $\beta = .8$ and $1/L = .001$ cm^2/g and assuming $\lambda = 200$ g/cm^2 we obtain:

$$\Lambda = (253 \pm 40) \text{ g/cm}^2$$

Here the error refers only to the uncertainty in β and $1/L$; it does not include possible error in the assumed value of λ. If $1/L$ is small, the value of Λ is essentially unaffected by errors in this quantity. Therefore, a rather crude demonstration that K is independent of x for constant N is sufficient to determine Λ with considerable precision.

In this way we have reduced the measurements of K vs θ for constant observed number of electrons to measurements of K vs θ for constant equivalent vertical size. Alternatively, it is possible to regroup the showers according to equivalent vertical size as defined by Equation III (10). If this is done, then K can be computed as a function of x for showers which do have nearly the same equivalent vertical size but come in at different zenith angles. Figure 12 shows the results of these computations. The abscissa is the depth x. The ordinates of the solid points are the values of K for constant equivalent vertical size as deduced from measurement on showers

with constant observed size. The ordinates of the open points are the measured values of K in showers with constant equivalent vertical size but different zenith angles. The solid lines were computed according to the formula

$$K = 39\ m^{-1} \left(\frac{N(x_0)}{10^6} \right)^{.79} e^{-\frac{(x-x_0)}{253\ g/cm^2}} \qquad \text{III} \quad (16)$$

where $N(x_0)$ is the equivalent vertical size. This formula summarizes our results for the dependence of K on N and x. In Figure 12 the fact that the values of K computed by two different methods agree, is further evidence for the validity of the procedure used to obtain Λ from measurements of λ, β, and L.

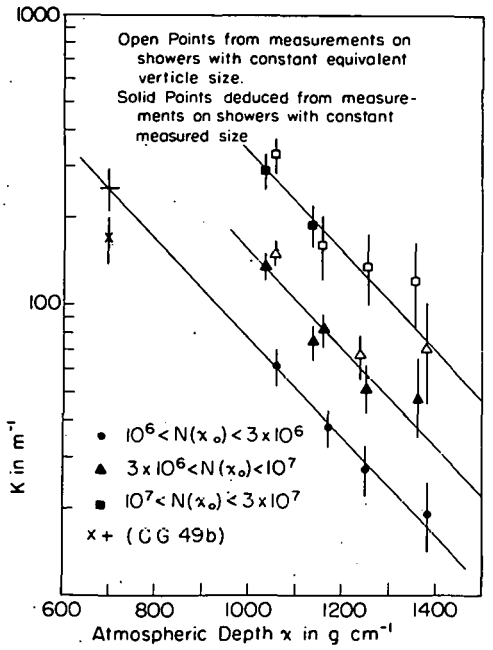

DEPENDENCE OF K ON DEPTH FOR CONSTANT EQUIVALENT VERTICLE SIZE

Figure 12

The values of K at x = 700 g/cm^2 were deduced from the measurements of Cocconi, Tongiorgi, and Greisen at mountain altitudes of the ratio of the density of mesons to that of electrons at 48 m from the core (CG 496). The method by which this was done will be explained in a later section.

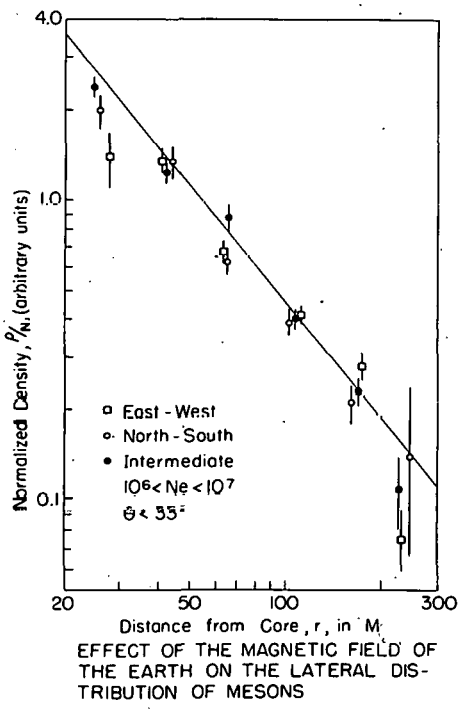

EFFECT OF THE MAGNETIC FIELD OF THE EARTH ON THE LATERAL DISTRIBUTION OF MESONS

Figure 13

C. Effect of the Magnetic Field of the Earth on the Lateral Distribution

It is possible that the magnetic field of the earth might deflect the mu-mesons in showers enough so that an effect would be observable. We would expect the horizontal North-South field of the earth to deflect vertical mesons to the East and West thus producing higher densities East-West of the core than North-South of it.

In Figure 13 are plotted the results of an attempt to detect such an effect. All the showers observed with the hodoscope in position A were sorted into three groups according to the azimuth of their cores with respect to the detector. "North-South" and "East-West" showers hit in the four 60° sectors centered N-S and E-W, respectively, and "Intermediate" showers hit in the four 30° sectors between the N-S and E-W areas.

Figure 13 presents the lateral distributions for showers in these three groups which also have $\theta < 33°$ and $10^6 < N_e < 10^7$. ρ/N has been used as the ordinate in order to eliminate any azimuthal variations in the mean size arising from the fact that the meson detector was not in the

exact center of the air shower array. It is apparent from the figure that there is no great difference between the three curves. We estimate from the errors on the individual points that it is very unlikely that the true NS and EW curves could be displaced from one another by more than 20% at $r = 100$ m.

D. The Rate of Absorption of the Mesons in Lead

We can obtain some information on the energy spectrum of the penetrating particles by measuring the average number absorbed in the lead between the two hodoscope trays. If there were no absorption or local production of any kind and if the trays were identical in every respect, then the total number of discharges in the top and bottom trays would be equal. Therefore, we can interpret any excess of discharges in the top tray as evidence for absorption in the lead between the trays provided that the other assumptions are still valid. This excess is likely to be subject to large statistical errors, because, in inclined showers, fluctuations in the numbers of mesons that hit one tray but miss the other may be much larger than the true excess. Errors due to this source can be reduced by decreasing the distance between the trays and by requiring that the zenith angles of the showers be small. These absorption measurements are also subject to large systematic errors arising from small differences in the efficiency of the two trays.

In order to verify that the two trays were equally efficient, the hodoscope was triggered with a Geiger tube telescope consisting of two 48" Geiger tubes, each of which was placed directly on top of the tubes in one of the trays with its length perpendicular to their axes. Since any particle which triggered this telescope also went through both trays, any inequality in the efficiencies of the two trays should cause an excess of unaccompanied discharges in the more efficient tray. In Table V, the events in two telescope runs have been categorized according to the number of tubes discharged in each tray. In the October 13 run it is clear that, within the accuracy of the statistics, the numbers of unaccompanied discharges in Tray A and in Tray B are equal. Since the total number of mesons traversing the trays was about 500 and since a difference of about 10 in the number of accompanied discharges in Tray A and Tray B would be statistically significant, we could easily detect a 2% difference in the efficiencies of the two trays. In the December 10 run, on the other hand, it appears that Tray A was about 4% more efficient than Tray B. This figure is probably about the worst assymetry that ever existed because, at the time of the run, the Geiger tubes had deteriorated to such a degree that they were just about due to be replaced. A correction based on this 4% difference was applied to all the absorption data taken with the hodoscope in this condition. All the rest of the data were taken while the trays were equally efficient.

TABLE V

OCTOBER 13, 1956

Number of tubes discharged in Tray B	Number of tubes discharged in Tray A			
	0	1	2	3
0	3	18	1	
1	21	410	41	5
2		36	14	3
3		8		

Total number of events = 560

DECEMBER 10, 1956

Number of tubes discharged in Tray B	Number of tubes discharged in Tray A			
	0	1	2	3
0	4	16	4	
1	10	200	30	4
2		31	7	1
3		1		1

Total number of events - 309

In Figure 14 we consider the dependence of the absorption on the distance from the core. The abscissa is the distance from the core r and the ordinates of the solid points are the quantities:

$$F = \frac{N_A - N_B}{N_A\, p(\theta)} \qquad \text{III} \quad (17)$$

where, for each radial group, N_A and N_B are the total number of discharges in the top and bottom trays, respectively, and $p(\bar{\theta})$ is the probability that a particle which hits the top tray will also hit the bottom tray. Since $N_A - N_B$ is presumably the number of mesons stopping in the absorber and $N_A\, p(\bar{\theta})$ is the number of mesons going through both trays, F can be interpreted as the fraction of the mesons reaching the top tray that stop in the absorber between the trays. The zenith angles of the showers used for this plot were all less than 25°. The errors, which are much smaller than they would be if N_A and N_B were statistically independent, were calculated using a formula derived in an Appendix.

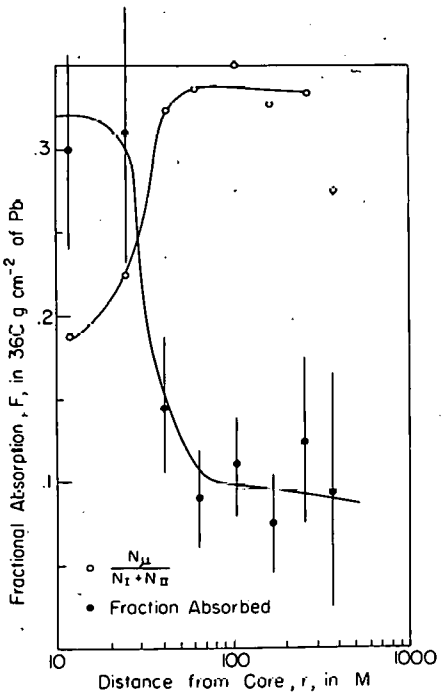

RADIAL DEPENDENCE OF THE FRACTIONAL ABSORPTION

Figure 14

On this figure we see that the apparent absorption amounts to 30% near the core but drops to only 10% in the region $r > 50$ m. This nearly discontinuous transition followed by a region of constant absorption can be interpreted as an effect caused by the nuclear active component of the shower. Presumably secondary particles of local interactions produced in the lead by the nuclear active particles are much more strongly absorbed than mu-mesons incident from the air. This would explain the strong absorption in the region where nuclear active particles are known to be concentrated. As further evidence for the validity of this interpretation, we have plotted as open circles on Figure 14 the quantity:

$$G = \frac{N_{\mu}}{N_A + N_B} \qquad \text{III} \quad (18)$$

This quantity is a measure of the fraction of the total number of discharges which can be associated with mu-mesons identified by interpreting the hodoscope pictures. If the number of discharges is small enough so that the hodoscope records can always be satisfactorily interpreted, this quantity should be a constant if all the discharges were caused by mu-mesons. Since the total number of discharges was always rather small, we feel that the sharp drop in G at small radii is evidence for a large number of multiple discharges associated with nuclear interactions.

If we interpret the constant absorption at large distances as absorption of mu-mesons we obtain the result that the range spectrum is independent of radius for $50 \text{ m} < r < 400$ m and that the fraction of mesons with ranges greater than 540 g/cm^2 of Pb which are absorbed in an additional 360 g/cm^2 of Pb is $9.9\% \pm 1.5\%$.

E. Dependence of the Ratio of the Meson Density to the Total Density on Distance to the Core

A quantity which has been measured in other experiments is R_p, which is the ratio of the density of penetrating particles to the density of all charged particles. In order to compare the present results with other experiments we have derived values of R_p based on our measured densities of penetrating particles and on measurements of the total density made with the air shower detectors.

Comparison of Geiger and Scintillator Densities

Since most previous measurements of air shower electron densities have used Geiger tubes, we have made a direct comparison of the densities measured by the scintillation counters and the densities measured with the unshielded hodoscope trays operated in position A. The two trays were placed side by side with nothing but the roof of a tent above them, and a standard air shower scintillation detector with area 1 m^2 was set up about 2 m from the trays. The triggering requirement used was the normal one for studying air showers.

The Geiger tube density measurements were based on the same type of analysis that was used to relate density of penetrating particles to the number of tubes discharged in the bottom tray (see Section III B). In this case, however, densities were inferred directly from the expression:

$$\bar{n} = 96\,(1 - e^{-\bar{\rho}A}) \qquad \text{III (19)}$$

where $\bar{n}$ is the mean number of tubes discharged per shower, $\bar{\rho}$ is the average density of the showers, A is the area of a single tube, and 96 is the total number of tubes used. In principle, one should take into account the a priori probability distribution of ρ in determining the true average density. However, the average value of the quantity $1 - e^{-\rho A}$ is very nearly equal to the quantity $1 - e^{-\bar{\rho}A}$, where $\bar{\rho}$ is the true average density, provided that ρA is restricted to sufficiently small values. This condition has been satisfied by restricting the values of ρ used in the final comparison to $\rho < 40$ p/m^2. This value of ρ corresponds to $\rho A = 1.06$. The densities measured by Geiger tubes for $\rho > 40$ p/m^2 may be very slightly in error due to the crudeness of this analysis, but a more complete analysis is not necessary for the small amount of data obtained with

$\rho > 40$ p/m^2. A cosmic ray telescope was used to calibrate the scintillation counters under the assumption that the mean pulse height produced by vertical cosmic rays unassociated with showers is the same as the mean pulse height per particle in air showers. A detailed examination of the hodoscope records showed that the error due to two tubes being discharged by one inclined particle was negligible.

Table VI summarizes the results of the comparison of the Geiger tube and scintillation counter density measurents. In Table VI the showers have been classified according to the values of the density at position A. In this classification the density ρc was obtained from an assumed structure function fitted to the densities measured by the scintillation detectors in the regular air shower array. Therefore, ρc is an interpolated density which reflects the average calibration of all the detectors in the array. Since the detectors at position A were included in neither the triggering nor the fitting, ρc is not directly affected by the measurements made with the two detectors at position A.

From Table VI we can see that there is a systematic difference between the interpolated density ρc and the directly measured density ρs. This difference can be attributed to errors in the calibration of the scintillation counter. Since the evaluation of ρc involves an average over the data from many detectors, it is the most suitable quantity for comparison with the densities measured with the Geiger tubes. From Table VI we see that the ratio $\rho G/\rho c$ is approximately independent of the value of ρc and that the average ratio for $\rho_c < 40$ p/m^2 is $1.3 \pm .1$. The statistical uncertainties in ρ_G and ρ_c contribute little to the error in this quantity. Most of the uncertainty is due to systematic calibration errors, which we estimate could be as large as 10%.

Determination of R_p

Figure 15 shows the results of the determination of the ratio of mu-meson density to the total density of charged particles. For the total density we have used the following approximation to the Nishimura-Kamata (GK 56) lateral distribution for $s = 1.4$:

$$\rho(r) = \frac{Ne}{2\pi r_o} \quad \frac{1.15}{r} \quad \left(\frac{2}{2 + r/r_o}\right)^{3.3} \qquad \text{III} \quad (19)$$

TABLE VI

Range of ρc	Mean Interpolated Density	Mean Density Measured by Scintillator	Mean Density Measured with Geiger Tubes	Mean Number of Geiger Tubes Discharged				Number of Showers in Groups
	ρ_c	ρ_s	ρ_G	$\bar{N}$	ρ_G/ρ_c	ρ_G/ρ_s	ρ_s/ρ_c	
0-5	3.9	3.2	5.8	13.9	1.49	1.84	.815	8
5-10	7.5	6.6	9.2	21.0	1.23	1.41	.870	24
10-20	13.1	12.0	16.3	33.8	1.24	1.36	.915	24
20-30	24.1	23.4	32.2	55.5	1.34	1.38	.975	14
30-40	33.0	30.0	43.1	65.	1.31	1.41	.90	4
40-50	44.1	44.2	66.6	79.7	1.51	1.51	1.00	10
50-70	60.6	63.2	68.0	80.5	1.12	1.07	1.04	5
Combined Results					1.30	1.42	1.10	89

where $\rho(r)$ is the electron density at distance, r, r_o is 79 m, N is the total number of particles, and r is measured in meters. This expression accurately expresses the results obtained from the air shower experiment for $r < 300$ m. The ordinates of the points on Figure 15 for $r < 400$ m are the ratio of measured values of the mu-meson density for vertical showers as obtained from Figure 8 to the total density computed from Equation III (19). The point at 850 m is based on an independent measurement of the total density at this distance made with the unshielded Detector II trays. Since the triggering requirements were identical for the shielded and the unshielded runs, the ratio R_p is given by:

$$R_p = 1.3 \frac{n_s}{N_s} \frac{N_u}{n_u} \qquad \text{III} \quad (20)$$

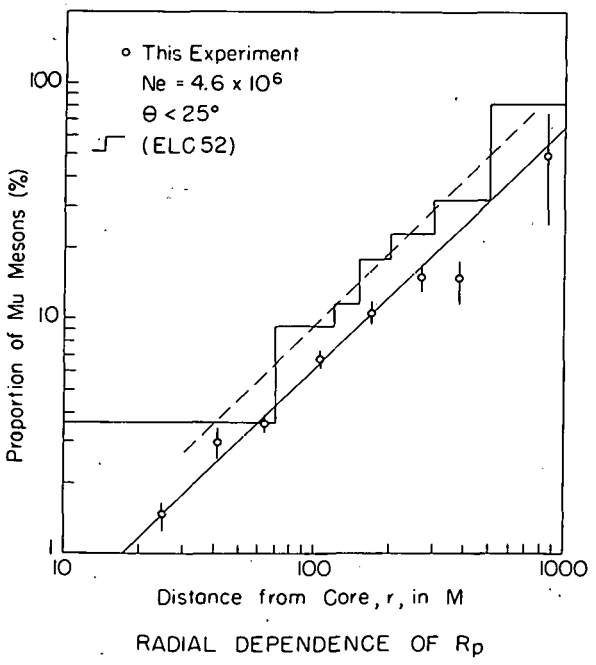

RADIAL DEPENDENCE OF R_p

Figure 15

where n_s/N_s and n_u/N_u are, respectively, the fraction of the showers observed which had a count in the distant detector with the trays shielded and the same fraction with the trays unshielded. The factor of 1.3, which is the ratio of Geiger-tube densities to scintillation densities, has been included in order to bring this value of R_p into harmony with the values obtained at other values of r which are all based on scintillation counter density measurements. The zigzag line presents the measurements of Eidus et al (ELC 52) of R_p as a function of distance from the core. The values of R_p quoted by Eidus have been multiplied by the factor 1.3 since these measurements were based on Geiger counter total density measurements.

From our measured values of R_p we obtain the result:

$$R_p \propto r^{1.0 \pm .1}$$

This result is consistent with the measurements of Eidus, but there is a discrepancy of about a factor of 1.4 between the absolute values of R_p obtained in the two experiments.

E. Comparison with Other Experiments

The only results on the lateral distribution of μ-mesons which are directly comparable with the results of the present experiment are those of Porter and Sherwood (PNA 57). In Figure 15a the dashed line is their measured lateral distribution for showers of mean size 6×10^6 electrons which came in at all zenith angles. The solid line is our lateral distribution for showers of mean size 4×10^6 electrons which came in with $\theta < 25°$. Since the ordinate is ρ/N, the difference in shower sizes has been approximately taken into account and the curves would coincide if the agreement were perfect. It is apparent that the curves do not coincide. Furthermore, since the magnitude of the discrepancy depends upon the distance to the core, the disagreement cannot be removed by multiplying one curve or the other by a constant factor. Such a factor would be easy to explain, because it could be attributed to errors in the shower size determination or other errors that are independent of the core distance.

The difference between the two curves can be attributed to two effects, both of which are connected with the fact that Porter and Sherwood were not able to determine the zenith angles of the showers they observed. In the first place, we have seen in Section III A that the density at large distances from the core increases more rapidly with zenith angle than does the density near the core. Since the average zenith angle for all showers is certainly larger than the average zenith angle for showers restricted to $\theta < 25°$, we would expect the dashed curve to lie above the solid curve at large distances from the core. In the second place, the distances from the core used by Porter and Sherwood were measured in the plane of the experiment whereas the distances used in the present experiment were all measured in a plane perpendicular to the shower axis. Since the distance in the plane of the array is always greater than the distance in the perpendicular plane, the effect of averaging over arrival directions is to make the distances measured by Porter and Sherwood greater than the average distances which would be measured in our reference system. This effect is also in the right direction to explain the observed discrepancy.

The discrepancy with the results of Porter and Sherwood is not connected with our procedure for interpreting hodoscope records, because, at all distances to the core, the lateral distribution based on densities deduced from the number of tubes discharged in the bottom tray is

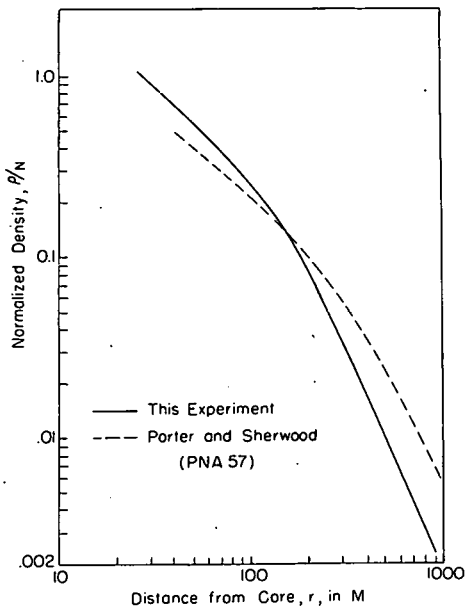

Figure 15a

identical to the lateral distribution based on interpretation of hodoscope records except for a constant factor which can be attributed to knock on electrons.

The factor of 1.4 difference between our values of R_p and those of Eidus et al (see Figure 15) can also be explained by the considerations presented above. It is worth noting that this discrepancy is statistically significant only at large distances from the core.

IV. INTERPRETATION AND DISCUSSION OF THE RESULTS

A. Gross Facts

There are two basic characteristics of the mu-mesons in showers with interpretations that are essentially independent of the detailed nature of the shower development. These are (1) the large number of mesons in the showers and (2) the large root-mean-square radius of the meson lateral distribution.

The number of μ-mesons depends upon the numbers and energies of the π-mesons produced in nuclear interactions. The large number of μ-mesons implies that the number of μ-meson producing interactions is large. Even if we take a multiplicity of 200 π-mesons for every interaction (200 is approximately the multiplicity predicted by the Fermi theory (FE 50) for a nucleon-nucleon interaction of 10^{17} ev) and assume that all these π-mesons decay, the number of interactions inferred from the observed number of μ-mesons is greater than 2500 for a 10^7 electron shower. This number, which is a conservative lower limit, is much larger than the number of collisions a primary particle would make in going through the atmosphere. In fact, with a collision mean free path of 100 g/cm^2, the mean number of collisions such a particle would make is only 10.

Since it is very unlikely that the multiplicity of the average interaction is actually as large as assumed and since the other estimates involved in the calculation are conservative, it is likely that this lower limit on the number of interactions is much less than the actual number involved.* The only reasonable explanation of this large number of interactions is that there exists a nuclear cascade process in which each interaction produces several particles capable of producing further interactions. This cascade of secondary particles is not necessarily important in the development of the shower. For example, it could be that essentially all of the energy involved is carried away from an interaction by only one of the emerging particles. If this were true there would always be

---

* If the showers were caused by dust grains, as has been suggested by Alfven, the effective "multiplicity" in the first interaction might be very large. However, Porter and Sherwood (PNA 57) have shown that the proportion of μ-mesons in the central regions of the shower predicted by this model is about five times larger than the observed proportion and that, consequently, the model is incompatible with experimental results.

one particle with much higher energy than all the rest and the interactions of this particle would control the development of the shower. In this case, the large number of interactions needed to explain the large number of μ-mesons could occur in cascades, which involve a small fraction of the total shower energy, and which are generated by the secondaries with relatively low energy.

No matter how many particles carry the bulk of the energy in the shower, it is likely that most of the μ-mesons arise from interactions of such low energy that the average number of secondary particles which interact is on the order of one. This assertion is based on the assumption that the $\pi - \mu$ decay process is the main effect which tends to damp the development of the nuclear cascade and on the fact that, in any cascade of interactions, further increase in the number of interacting particles stops when the cascade reaches a stage where the mean number of interacting particles produced in each interaction is less than one. In such a cascade, the majority of the interactions tend to be those whose multiplicity of interacting particles is very near one. These properties are well known in the case of electronic cascade multiplication and it is easy to show that they are characteristic of any "damped" cascade.

We know from the results of experiments with accelerators (SRP 56) that the mean number of secondary π-mesons produced in nuclear interactions generated by particles with energies around 2 Bev is greater than one. Consequently, if the π-mesons did not decay, the multiplicities at these very moderate energies would be large enough to sustain the development of cascades. Since the average multiplicity certainly increases with energy, this same conclusion would be valid at any higher energy. Therefore, if it were not for the decay of π-mesons, the nuclear cascade would continue to grow even if the average energy of its participants were as low as 2 Bev. The effect of the $\pi - \mu$ decay is to decrease the effective multiplicity at all stages of the process because many of the π-mesons decay before they have a chance to interact. Since the probability that a 2 Bev π-meson interacts before decaying in air at sea level is on the order of .2, it is apparent that the $\pi - \mu$ decay is a much more important factor in the nuclear cascade in air than is the fact that the multiplicity drops below one at some energy which is less than 2 Bev.

The energy, which the effect of π decay prevents further cascade multiplication, can be estimated without detailed knowledge of the nature of the interactions. We shall assume that the

only products of the interactions are π-mesons. It can be shown that the probability that a π-meson of energy E interacts before it decays at atmospheric depth x is:

$$P_I(E,x) = \frac{\left(\frac{ct_0}{h_0}\right)\left(\frac{E}{Mc^2}\right)\left(\frac{x}{L}\right)}{1+\left(\frac{ct_0}{h_0}\right)\left(\frac{E}{Mc^2}\right)\left(\frac{x}{L}\right)} \qquad \text{IV} \quad (1)$$

where ct_0 is the distance a π-meson travelling at the velocity of light would go in one mean life (8 m), Mc^2 is the rest energy of the π-meson (141 Mev), h_0 is a characteristic length for the atmosphere (7 km) and L is the collision mean free path for the π's (100 g cm^{-2}). If we now let $n(E_0, E)\,dE$ be the mean number of π-mesons produced with energy E in dE in an interaction of primary energy E_0, the mean number of secondary π' s that will interact is:

$$n_I(E_0,x) = \int_0^\infty n(E_0,E)\; P_I(E,x)\,dE$$

$$= \left(\frac{ct_0}{h_0}\right)\left(\frac{x}{L}\right)\frac{1}{Mc^2}\int_0^\infty \frac{E\; n(E_0,E)\,dE}{1+\left(\frac{ct_0}{h_0}\right)\left(\frac{x}{L}\right)\left(\frac{E}{mc^2}\right)} \qquad \text{IV} \quad (2)$$

If the term $\left(\frac{c\tau_0}{h_0}\right)\left(\frac{x}{L}\right)\left(\frac{E}{mc^2}\right)$ is small compared to 1

throughout the range of E that contributed to the integral in IV (2), we may neglect this term in the denominator and obtain:

$$n_I(E_0) = \left(\frac{ct_0}{h_0}\right)\left(\frac{x}{L}\right)\left(\frac{E_\pi}{Mc^2}\right) \qquad \text{IV} \quad (3)$$

where E_π is the total energy going into π-mesons produced in the interaction. This result is interesting because, within the limits of its applicability, the only characteristic of the interaction which appears is E_π; neither the total multiplicity nor the distribution of energy among the π-mes-

ons are involved. Since one of the secondary mesons might conceivably be carrying most of the energy E_π, Equation IV (3) is strictly accurate only if the value of $n_I(E_0)$ is much less than 1. (It is likely that the energy is fairly evenly distributed among the secondary π-mesons for interactions of energies such that $n_i \gtrsim 1$. If this is the case, and if the total multiplicity is high, Equation IV (3) would be fairly accurate even if n_i were on the order of one.)

Since the value of $n_i(E_0)$ from Equation IV (3) is greater than the actual number which interact, and since the energy E_π is less than the total energy of the collision E_0, we can use IV (3) to set a lower limit on the energy E_c for which $n_i(E_c) = 1$. If we insert numerical values into IV (3) we obtain:

$$n_i(E_c) = \frac{x}{1030 \text{ g cm}^{-2}} \times \frac{E_0}{12 \text{ Bev}} \qquad \text{IV (4)}$$

where E_0 is measured in Bev and x in g/cm^2. This result implies that the mean energy of primaries that cause interactions for which $n_i(E_c) = 1$ is greater than 12 Bev at sea level and proportionally greater at smaller depths. Since the condition that $n_i(E_c) = 1$ is also the condition that cascade multiplication ceases, we would expect most of the interactions in the shower to have approximately this energy. If we now use the Fermi multiplicity of 4 for such collisions and assume that all four of the π-mesons eventually give rise to a μ-meson, we obtain from the number of μ-mesons in a 10^7 electron shower, 1.2×10^5 for the total number of interactions in such a shower. Since all the approximations on which this estimate is based tend to make it too small, this value is still a lower limit on the number of interactions. The most significant sources of uncertainty in the preceding discussion are (1) we have neglected decay and absorption of the μ-mesons before they reach the level of observation (2) we have used the number of μ-mesons falling within 900 m of the core -- not the total number. It is possible that these plus errors in our guess for the multiplicity might cause our estimate to be too low by as much as a factor of 10. Therefore, we have obtained the result that the total number of interactions in a 10^7 electron shower lies in the range 10^5 to 10^6 and that the average energy of the particles producing these interactions is in the range 10 to 100 Bev. The fact that the μ-mesons come from π-mesons produced in many interactions of relatively low energy means that little or no direct information can be obtained from the present experiment on interactions with energies comparable to the energy of the

primary. However, we can use knowledge of the μ-component as a means of studying the development of the shower and the development is certainly influenced by the characteristics of the interactions of the high energy particles in the shower. Furthermore, it is possible to obtain some information on the avarage angular distribution of π-mesons in interactions which have higher energies than are presently available from accelerators.

Interpretation of the Large Lateral Spread of the Mesons

One process that certainly helps cause the mesons to spread away from the core is multiple scattering. However, the magnitude of the observed spread rules out multiple scattering as the main source of spread. In Table VII we present the calculated value of the root-mean-square radius expected from multiple scattering for mesons which are produced with just enough energy to go through the rest of the atmosphere and through the 400 g cm^{-2} of lead above our meson detector (Detector II). From this table we see that even if all the mesons were produced at a depth of 100 g cm^{-2} (which is unlikely, because at that depth only one generation of particles is involved) it would be impossible to account for our observed lower limit on the r.m.s. radius, which was ~330 m. If we consider the fact that this lower limit is almost certainly much less than the true r.m.s. radius, then it appears that multiple scattering is completely ruled out as the main source of the lateral spread.

A similar argument applies to the lateral spread which occurs because the trajectories of the decay μ-mesons make a finite angle with the direction of the decaying π-mesons. Table VIII presents the maximum lateral displacement expected from this effect for mesons which are produced with just enough energy to set off the meson detector. The computations of these displacements were based on the fact that the maximum momentum of a decaying meson perpendicular to the direction of the π-meson is 30 Mev. Since the figures in the last column are all less the lower limit on the r.m.s. radius and since the r.m.s. radius corresponding to the r.m.s decay angle is certainly less than the maximum displacement, this effect is also ruled out as the main source of lateral spread.

The only other process which could lead to the observed spread is the angular spread of the π-mesons at production. In attempting to explain the shape of the lateral distribution, we will

assume that this is the only cause of the spread.

TABLE VII

Depth of Origin	Energy at Origin	Root-Mean-Square Radius
0 g cm^{-2}	2.5 Bev	430 m
100	2.3	300
200	2.1	240
400	1.6	180
600	1.2	110

TABLE VIII

Depth of Decay	Energy at Decay	Maximum Lateral Displacement
100 g cm^{-2}	2.3 Bev	215 m
200	2.1	170
400	1.6	140
600	1.2	110

B. Interpretation of the Shape of the Lateral Distributions

We have seen that the μ-mesons in air showers result from the decay of π-mesons produced with a significant angular spread in a multitude of nuclear interactions. We will now attempt to say something about where these interactions occur and what the magnitude of the angular spread is. We will do this by comparing the observed lateral distributions with those computed under the assumption that all the interactions occur on a line at the center of the shower and that the angular distribution of the μ-mesons arising from these interactions is independent of the depth at which they occur.

The first of these assumptions is probably rather well justified because the nuclear active component of showers is known to be concentrated near the shower axis (DNA 56). The second is not so well founded because Equation IV (4) implies that the energy of the average interaction increases with decreasing depth so that the average angle is presumably smaller for the interactions occurring at small depths. Nevertheless, we shall retain this simplifying assumption because the error which it introduces is small compared to other uncertainties in the analysis. We have also assumed that the angular spread of the μ-mesons arising from interactions is large compared to the angles which the trajectories of the parent π-mesons make with respect to the direction of the shower axis. This assumption is probably well justified because the high energy, well collimated particles emerging from an interaction are the ones which produce further interactions.

In order to compute lateral distributions under these assumptions we need to know two things:

(1) The number of μ-mesons produced at each depth

(2) The angular distribution of the μ-mesons

If these are given, it is a simple matter to express the lateral distribution as an integral over the depth. Since, in fact, neither (1) nor (2) is known, our program will be to compute lateral distributions under a variety of assumptions for the depth and angular distributions of the μ-mesons and to see which assumptions (if any) are incompatible with the observed lateral distributions.

By this procedure we should be able to set rough limits on the class of angular and depth distributions that are compatible with the experimental results.

We shall assume that the number of mesons produced at a depth x in the depth increment dx is given by:

$$dN(x) = G(x)\,dx \qquad \text{IV (5)}$$

In evaluating the integrals, it is convenient to normalize G so that the total number of mesons produced at all depths is 1 and to use the variable $u = x/x_o$ where x_o is the total thickness of the atmosphere above the level of observation. We then have:

$$dN(u) = g(u)\,du \qquad \text{IV (6)}$$

for the number of μ's produced at u in the increment du.

We shall assume that the small angle approximation is valid and that the angular distribution is described by:

$$p(\theta)\,d\omega = \frac{1}{2\pi\theta_o^2}\, f\left(\frac{\theta}{\theta_o}\right)\, d\omega \qquad \text{IV (7)}$$

where $p(\theta)\,d\omega$ is the probability that a meson is emitted within the solid angle element $d\omega$ at an angle θ, θ_o is the root-mean-square angle of the distribution and $f\left(\frac{\theta}{\theta_o}\right)$ is a function which has been normalized so that $\int_o^\infty t\, f(t)\,dt = 1$. It can easily be verified that the requirement that $\int_o^\infty 2\pi\theta p(\theta)\,d\theta = 1$ is satisfied for this definition of $p(\theta)$.

With these definitions we find that the density produced at a distance r from the core by the mesons originating in dx at x is:

$$d\rho(r) = dx\; G(x) \frac{1}{[h(x)]^2}\; p\left(\frac{r}{h}\right) \qquad \text{IV (8)}$$

where h is the distance to the level of observation from the level of depth x. Equation IV (8) is a direct consequence of the fact that the solid angle subtended at the source by a detector of area A located at the level of observation is $d\omega = A/h^2$ and that the angle a meson must have in

order to reach distance r starting at a distance h is $\theta = r/h$. An integral over x yields the total density at the distance r:

$$\rho(r) = \int_0^{x_0} \frac{G(x)_2}{[h(x)]} \quad p\left(\frac{r}{h(x)}\right) dx \qquad \text{IV (9)}$$

For an exponential atmosphere, $h(x)$ is given by:

$$h(x) = h_0 \log \frac{x_0}{x} \qquad \text{IV (10)}$$

where h_0 is a characteristic length for the atmosphere (7 KM). If we use this expression for h and rewrite IV (9) in terms of the functions g and f we obtain:

$$\rho(r) = \frac{1}{2\pi(h_0 \theta_0)^2} \int_0^1 \frac{g(u)\,du}{[\log u]^2} \quad f\left(\frac{r}{h_0 \theta_0 \log u}\right)$$

If we now set $h_0 \theta_0 = r_0$ we obtain the result: IV (11)

$$2\pi r_0^2 \rho\left(\frac{r}{r_0}\right) = \int_0^1 \frac{g(u)\,du}{[\log u]^2} \quad f\left(\frac{r/r_0}{\log u}\right)$$

This is the quantity which will be plotted in graphs presenting computed lateral distributions.

We shall use the following three functions, which are plotted in an insert on Figure 16, as trial functions for $g(u)$:

$$(1) \qquad g_1(u) = 10 \frac{(10u)^8 e^{-10u}}{8!}$$

$$(2) \qquad g_2(u) = 10 \frac{(10u)^5 e^{-10u}}{5!} \qquad \text{IV (12)}$$

$$(3) \qquad g_3(u) = 10 \frac{(10u)^2 e^{-10u}}{2!}$$

These functions have been normalized so that $\int_0^\infty g(u)\,du = 1$. They were selected so that the maximum production would occur at 800 g/cm^2 (1), 500 g/cm^2 (2) and 200 g/cm^2 (3).

For the angular distribution function $f\left(\frac{\theta}{\theta_0}\right)$ we shall use:

$$f_1\left(\theta/\theta_0\right) = \begin{cases} 1 & \theta/\theta_0 < \sqrt{2} \\ 0 & \theta/\theta_0 > \sqrt{2} \end{cases}$$

and

$$f_2\left(\theta/\theta_0\right) = \begin{cases} \dfrac{1}{\sqrt{3}\,(\theta/\theta_0)} & \theta/\theta_0 < \sqrt{3} \\ 0 & \theta/\theta_0 > \sqrt{3} \end{cases} \qquad \text{IV (13)}$$

These functions, which have been chosen so that the r.m.s. angle is θ_0, have a sharp cut-off for angles larger than a certain critical angle. The function f_1 is flat at the origin. This is in accord with the evidence from individual stars detected in nuclear emulsions which seem to have angular distributions which are flat at the origin (CU 50). The function f_2 has a θ^{-1} singularity at the origin which was suggested by the observed r^{-1} lateral distribution. This choice is not incompatible with the emulsion evidence because the contributions from many interactions distributed over a broad range of energies might well add up to give a θ^{-1} angular distribution.

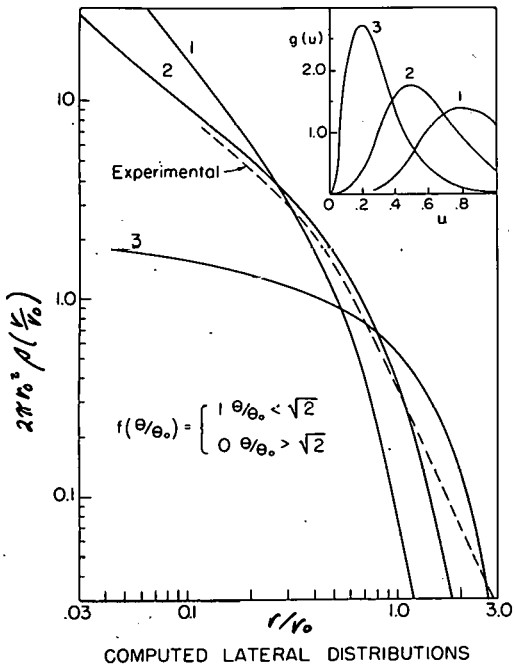

COMPUTED LATERAL DISTRIBUTIONS

Figure 16

Figure 16 shows the lateral distributions computed from Equation IV (11) using f_1 and each of the three $g(u)$'s. In attempting to fit these curves to the experimental lateral distribution it is permissible to adjust the abscissa as well as the ordinate because we have no a priori knowledge of the value of θ_0. It is apparent that the shape of the curve for $g_3(u)$ is incompatible with the shape of the experimental curve. The curves for $g_1(u)$ and $g_2(u)$ can be fitted reasonably well to the observed lateral distribution although the g_1 curve is a little too steep near the origin and the g_2 curve is a little too steep far from the origin. These discrepancies can be eliminated by slight modifications of the function $f\left(\frac{\theta}{\theta_0}\right)$. If we compute the values of θ_0 needed to give reasonably good fits to curves 1 and 2 in Figure 16, we obtain 14° and 2°, respectively.

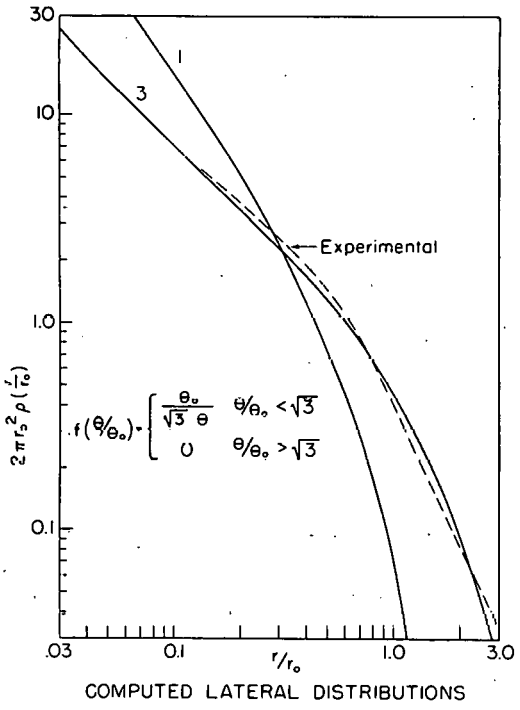

COMPUTED LATERAL DISTRIBUTIONS

Figure 17

Figure 17 shows the lateral distributions computed using f_2 and g_1 and g_3. These curves are similar in shape to the curves in Figure 16 and to the experimental curve. It is apparent that the use of a θ^{-1} angular distribution has eliminated the disagreement with experiment which we obtained with the flat angular distribution and $g_3(u)$. The values obtained for θ_0 are 13° for curve 3 and 2° for curve 1.

Since it is likely that at least one of the assumed g(u)'s is a rough approximation to the true production function for μ-mesons and since all the values of θ_0 deduced under our assumptions on f and g lie within the range 2° to 14°, the true value of θ_0 probably lies within this range. In a later section we will show how some information on g(u) can be obtained and used to make a better estimate of θ_0.

It is clear that the experimental results are compatible with a wide range of choices for f and g. The form of the function f is by no means restricted to the ones we have used. Agreement with experiment could undoubtedly be obtained for $f \alpha \theta^{-n}$ for any n between 0 and 1. However, it is unlikely that n could be as large as 2.

The next step is to try to eliminate some of the possibilities by the use of our experimental information on the change of the shape of the lateral distribution with zenith angle. Equation IV (11) can be used directly for the computation of lateral distributions in showers inclined at the angle θ provided we substitute $h_0/\cos\theta$ for h_0 and $x_0/\cos\theta$ for x_0 in the definition of u.

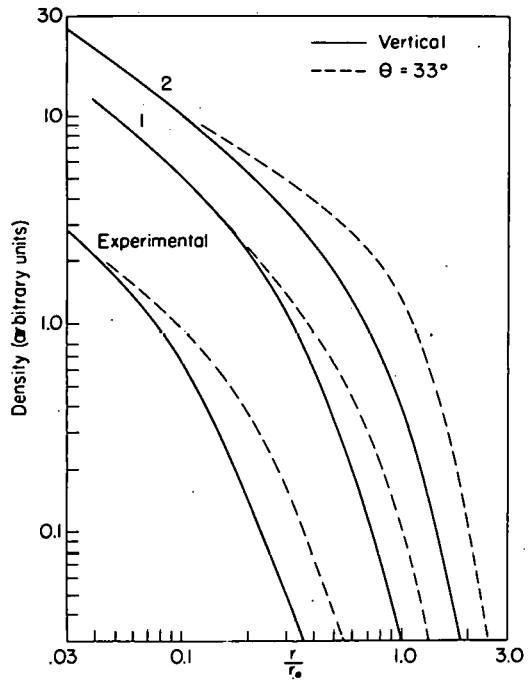

Figure 18

Figure 18 shows the lateral distributions obtained for showers coming in at an angle of 33° for production functions corresponding to g_1 and g_2. (The substitution $x_0(33°) = x_0(0°)/\cos 33°$

has been made in the definition of u.) The value of the unit in which distances are measured, r_o, is the same as the one used for vertical showers, so that the curves for vertical (solid line) and inclined (dashed line) showers are directly comparable. The ordinates of corresponding curves for different angles have been normalized so that the curves coincide at small values of r/r_o. The angular distribution function used was f_1.

It is apparent that the curves for g_2 show a larger change with angle than do those for g_1. It also appears that the experimental change is better described by the results for g_2 than by those for g_1. If this fact were taken seriously, it would imply that the production of mesons is not concentrated in the lower atmosphere; however, neither the experimental data nor the theoretical analysis are accurate enough for us to base a firm conclusion on this fact.

While the fact that the lateral distribution is more spread out for inclined showers does not put very stringent limitations on the functions f and g, it does tell us that the shape of the μ-meson lateral distribution depends upon the history of the shower. This behavior contrasts with the electron lateral distribution, the shape of which depends only on the characteristics of the air at the point of observation.

C. Interpretation of the Dependence of the Density Near the Core on Depth

In Section III (B) it was shown that, in showers of constant equivalent vertical size, K (see Equation III (16)) decreases exponentially with depth with an "absorption length" Λ of 253 g/cm^2. The processes which might cause such a decrease in the density near the core are (1) decay of the μ-mesons, (2) absorption in the air, and (3) increase in spread due to angular divergence. In addition to these processes leading to a decrease in the density near the core, there is production of new μ-mesons which would tend to cause an increase. Since the discussion which follows is concerned with the large magnitude of the decrease, the presence of production would only tend to strengthen the arguments.

Absorption can be ruled out because of the weak absorption observed in lead (see Section III (D)). If absorption were the main cause of the decrease we would expect the absorption in the 360 g/cm^2 of lead between the trays to be the same as the absorption in an equivalent thickness of air (200 g/cm^2). In fact, the absorption in the lead was only 9.9% (see Section III (D)) while the absorption in 200 g/cm^2 of air as deduced from Figure 12 was a factor of 2.2.

If the angular spread of the mesons is the main cause of the decrease, then we can deduce that the bulk of the mesons are <u>not</u> produced at small depths, If the meson production function were peaked at small depths ($g_3(u)$ of Equation IV (12) is an example of such a function) then it is necessary to assume that the angular distribution function is sharply peaked at small angles (f_2 of Equation IV (13) is an example of such a function) in order to explain the r^{-1} dependence of the lateral distribution near the core. With such a combination of f and g, the μ-mesons observed near the core at sea level are in a well collimated beam which suffers little decrease in intensity due to the angular spread of the mesons. In fact, under the assumption that all the mesons are produced at exactly 200 g/cm^2, it is easy to show that the expected decrease in density when the zenith angle is changed from 0° to 33° is only 25%, while the observed decrease for the same change in angle is about a factor of 2. Therefore, if the production is concentrated at small depths, decay of the mesons in flight is the only process which could result in the observed decrease in density near the core with increasing zenith angle.

If the observed decrease in the density near the core is to be explained as a consequence of the angular spread of the mesons, a large fraction of the mesons must be produced deep in the atmosphere (500 g/cm^2). Since it is likely that the production is spread over a wide range of depths, there is probably significant production even at sea level. We will show that, under the assumption that there is appreciable production at the level of observation and that the angular distribution of mesons is flat at small angles, K is a measure of the amount of meson production at the level of observation. Under the assumption that $f\left(\frac{\theta}{\theta_o}\right) = f_1$ (see Section IV B), Equation IV (11) gives :

$$2\pi r_o^2 \rho(r) = \int_o^{e^{-r/r_o\sqrt{2}}} \frac{g(u)\,du}{[\log u]^2} \qquad \text{IV (14)}$$

If we now split the integral into two parts -- an integral from $u = 0$ to $u = u_o$ and an integral from u_o to $e^{-r/r_o\sqrt{2}}$ where u_o is an arbitrary value which is close to 1 but less than $e^{-r/r_o\sqrt{2}}$ -- and if we assume that r is much less than r_o, we obtain:

$$2\pi r_o^2 \rho(r) = H(u_o) + \int_{u_o}^{1-r/r_o\sqrt{2}} \frac{g(u)du}{[\log u]^2} \qquad \text{IV (15)}$$

where $H(u_o)$ is a function of u_o. Transforming the variable of integration to $v = 1 - u$ and using the approximation $-\log(1 - v) = v$, which is valid for small v, we obtain:

$$2\pi r_o^2 \rho(r) = H(u_o) + g(1) \int_{r/r_o\sqrt{2}}^{1-u_o} \frac{dv}{v^2} \qquad \text{IV (16)}$$

where we have been able to take $g(1)$ outside the integral because of the assumption that $g(u)$ does not change much in the range $u = u_o$ to $u = e^{-r/r_o\sqrt{2}}$

Evaluating the integral in IV (16) we obtain :

$$2\pi r_o^2 \rho(r) = \tilde{H}(u_o) + g(1)\,\frac{r_o\sqrt{2}}{r} \qquad \text{IV (16a)}$$

Since the function $\tilde{H}(u_0)$ is independent of r, there is always a region near r = 0 where the term $\frac{r_0\sqrt{2}}{r} g(1)$ is much larger than $\tilde{H}(u_0)$ and in which, therefore, $\rho(r) \propto r^{-1}$. Since a similar argument would apply to other forms for $f(\theta/\theta_0)$ provided that they are flat at small values of θ, this result is interesting because it gives an explanation of the observed r^{-1} dependence of the lateral distribution under rather loose assumptions about the functions f and g. The only essential feature of the model is that there is a line source of mesons with significant production at the level of observation. The quantity g(1) appearing in Equation IV (16) is proportional to the production function at the observation level. The value of K deduced from IV (16a) is:

$$K = \frac{\sqrt{2}}{2\pi} \times \frac{x\, G(x)}{h_0 \theta_0} \qquad \text{IV (17)}$$

where G(x) is the number of mesons produced per g/cm^2 at depth x.

If we accept this interpretation of K, it is possible to use the experimental results on the variation of K with depth in order to obtain some information on the function G(x). In order to obtain the depth variation of K for depths less than 1030 g/cm^2 we shall extrapolate the exponential dependence which was presented in Section III (B) for depths greater than 1030 g/cm^2.

The value of K deduced from the measurements of Cocconi, Tongiorgi, and Greisen (CG 49a) is in good agreement with the results of this extrapolation. (See Figure 12.) These measurements gave the result that the density of penetrating particles near the core decreases by a factor of 2.33 ± .1 between the 710 g/cm^2 level and sea level in showers which had the same rate (and consequently the same primary energy) at the two elevations. The point marked by X in Figure 12 is the value of K deduced by multiplying the value of K obtained for vertical showers at sea level by this factor. In Equation IV (17) the factor x_0/h_0 is the density of air at the level of observation which, of course, is independent of the zenith angle of the showers. Therefore, the values of K obtained from inclined showers observed at sea level are directly proportional to the value of G(x). The value of K at 710 g/cm^2 must be multiplied by the factor 1030/710 in order to correct for the difference in air densities at the two altitudes. The point marked + in Figure 12 is the result of doing this.

It is apparent from Figure 12 that $G(x)$ decreases exponentially with depth over the range $700\ g/cm^2 < x < 1300\ g/cm^2$ for showers with a constant vertical size of 2×10^6 at sea level. The "absorption length" of this dependence is $253\ g/cm^2$ which, ofcourse, is the value of Λ which was deduced in Section III (B). This dependence of $G(x)$ on depth is very similar in form to the exponential dependence of the number of electrons in a shower of given primary energy on depth. In the first case the absorption length is $253\ g/cm^2$ while in the second case the corresponding length λ is $200\ g/cm^2$. This difference between λ and Λ is to be expected because the energy carried by the nuclear active particles (which is presumably proportional to the number of electrons) should decrease more rapidly with depth than the number of nuclear active particles (which is proportional to the number of μ-mesons produced) because the mean energy of the particles probably decreases with depth (GK 57).

We shall now attempt to use the information we have obtained on the function $G(x)$ in order to make a more accurate estimate of the r.m.s. angle θ_0 of the π-mesons in the interactions from which most of the μ-mesons arise. Since there is no experimental information on the value of K at atmospheric depths much less than $700\ g/cm^2$, we shall assume that $G(x)$ behaves like the number of particles in a shower which goes through a broad maximum at about $500\ g/cm^2$. For the estimate of θ_0, we have drawn a "reasonable" curve for $G(x)$ which joins smoothly onto the measured exponential portion of the curve and which has a maximum at about $500\ g/cm^2$. We shall use f_1 as the angular distribution function. Since the shape of the assumed production curve happens to be very similar to that of $g_2(u)$ (see the preceding section), the computed lateral distribution is practically identical in shape to curve 2 in Figure 16. We have already seen that the value of θ_0 which gives the best fit to this curve is 2°.

This value of θ_0 can be subjected to a test which is based on the relation between $G(x)$ and K. If we rearrange the factors in Equation IV (17) and integrate, we obtain:

$$\int_0^{x_0} G(x)\,dx = N_\mu = \frac{2\pi}{\sqrt{2}}\,(h_0\theta_0) \int_0^{x_0} \frac{K(x)\,dx}{x} \qquad \text{IV (18)}$$

where N_μ is the total number of mesons in the shower. If we integrate over the "reasonable" curve and insert 2° for the value of θ_0, we obtain $N_\mu \approx 3 \times 10^5$ mesons in a vertical shower of 2×10^6 electrons observed at sea level. The measured number of mesons which fall within 900 m of such a shower is only about 10^5 but it is likely that the mesons falling further than 900 m from the core might bring the true total number up to 2×10^5. The good agreement between the value of N_μ deduced from measurements of K vs depth and the value from direct measurements is a strong argument in favor of the basic validity of a model in which mesons are produced throughout the atmosphere. Nevertheless, the details of this basic picture could undergo considerable modification without introducing disagreement with the experimental results. For example, decay and absorption have been neglected in the computation of the lateral distributions. If these were taken into account, the value of θ_0 might become larger. This can be seen from Equation IV (18). Since the integral over K is not affected by decay or absorption (the mesons produced near the level of observation have no opportunity to decay or get absorbed) and since N_μ refers to the total number of mesons produced in the shower, the value of θ_0 must be larger than the value obtained if the number of mesons observed at sea level is used for N_μ. For this reason, our estimate of 2° for θ_0 must be interpreted as a lower limit. Since it is known from our results at sea level (Section I (D)) and from experiments at mountain altitudes (GK 57) that the mesons are weakly absorbed, it is likely that their average energy is so high that decay and absorption are not important effects. Therefore, 2° is probably rather close to the true value of θ_0.

The value of θ_0 depends upon the energy of the interaction and upon the angles at which the π-mesons are emitted in the center of mass frame of reference. Since we have already made an estimate of the energies of the interactions (Section IV (A)), we can compare the value of θ_0 deduced from our measurements with the value expected from the known energy of the interactions. If we assume that the mesons in the center of mass co-ordinates are emitted forward and backward in two cones of half angle θ_1^* then the half angle of the narrow cone in the laboratory system θ_1 is approximately given by:

$$\tan\theta_1 = \sqrt{\frac{2MC^2}{E}} \tan\frac{\theta^*}{2} \frac{\sqrt{1+1/2\,\frac{MC^2}{E}}}{\left(1+\frac{MC^2}{E}\right)} \qquad \text{IV (19)}$$

where MC^2 is the rest energy of the struck nucleus and E is the total energy of the particle which produces the interaction. Assuming three nuclei are struck and using our estimate E = 20 Bev, we obtain $\theta_1 \approx .17\theta_1^*$. Since our estimate of 2° was for the r.m.s. angle, which is certainly larger than θ_1, we obtain the result that $\theta_1^* > 12^\circ$. The true value of θ_1^* could be considerably larger than 12° if the true angular distribution were much more spread out than the distribution f_1 which we have used. Furthermore, the possible sources of error in the method of estimating the energy of the interactions and in the method of obtaining θ_0 tend to give too small a value of θ_0. Consequently, it is likely that the value of θ_1^* is somewhat larger than our lower limit. However, it is unlikely that these errors could cause more than a factor of 2 or 3 difference in the estimate of θ_1^* so we have the result that $12^\circ < \theta_1^* < 36^\circ$. This indicates that, in nuclear interactions of energy around 20 Bev, the mesons in the center of mass co-ordinates are emitted preferentially in the forward and backward directions in the center of mass co-ordinates.

The model, in which the production of μ-mesons is distributed along a line source which extends through the whole depth of the atmosphere, appears to give a good qualitative explanation of the experimental facts. The r^{-1} lateral distribution near the core is explained as an essentially geometric property of the line source. The variation of K with depth is identified with the variation of the production function G(x) with depth. The increase in the lateral spread with increasing zenith angle is explained as a consequence of the angular divergence of the mesons which are produced at high altitudes relative to the observation level. The model also agrees with the view that the development of air showers is strongly influenced by a few high energy nuclear active particles whose interactions feed new energy into the electron and μ-meson components at all depths. Since there is considerable evidence for this view from the slow rate of decrease of the electrons with depth (GK 57), it is likely that our model based on an extended line source is essentially correct.

On the other hand, the experimental results on μ-mesons alone do not rule out the possibility that essentially all the mesons are produced at some small atmospheric depth. In this case the r^{-1} lateral distribution would have to be attributed to a θ^{-1} angular distribution of the mesons at production. The rapid decrease of K with increasing depth would be a consequence of the decay of mesons in flight. The increase of lateral spread with zenith angle is again explained

as a consequence of the angular spread at production.

There are experiments which could distinguish between these two possibilities. If the value of K at a certain depth for inclined showers observed at mountain altitudes were compared with the value of K for the same depth obtained from vertical showers observed at a lower altitude and if it were found that the two values were equal, then decay would be ruled out as the main cause of the decrease of K with depth. This conclusion follows from the fact that the mesons produced at a given depth in inclined showers traverse a longer path before reaching the level of observation than do those in vertical showers. If the meson production depends only on depth, this implies that mesons produced at a certain depth in inclined showers have a greater probability of decay than those in vertical showers. Consequently, if decay is an important effect, the value of K for an inclined shower at mountain altitudes should be smaller than the value of K for an equivalent vertical shower at a lower altitude. If decay were ruled out by the results of this experiment, then we could also rule out the model in which production is concentrated at high altitudes, because, in this model, it was necessary to assume that the decrease of K with depth was due to decay. If the two values of K obtained were equal (except for the correction for the difference in the air density at the two locations) the interpretation of K as a reflection of the production function would be supported. It is worth noting that this proposed experiment would not require a very elaborate array of electron detectors because, it would be sufficient for an excellent determination of K to locate the cores of showers falling within a circle of only 100 m radius around a penetrating particle detector. However, it is absolutely necessary that the array have some provision for the measurement of the zenith angles of individual showers.

Another experiment which might distinguish between the two possibilities would involve a measurement of the angle which μ-meson trajectories make with the direction of the shower axis. If the mesons are produced along a line source, the mesons near the core should make a much larger angle with the axis than that expected if the mesons are produced at very high altitudes. Since we have shown that even in the case of a line source the angle is only on the order of 2°, the arrival direction of the shower and the angles of the mesons would have to be determined to at least $\pm 1°$. Although this requirement is rather stringent, it should be possible to do the experiment using a cloud chamber to measure the meson directions and a fast timing apparatus to meas-

ure the air shower arrival directions.

It would be desirable to do an experiment similar to the present one at a higher altitude. Such an experiment not only would make it possible to compare values of K obtained in vertical showers at different altitudes with those obtained in inclined showers at one altitude, but also it would give detailed information on the lateral distributions at smaller depths. Comparison of these lateral distributions with those obtained at sea level would surely help to specify the production function and the angular distribution of the μ-mesons in air showers.

APPENDIX I

EXPERIMENTAL DETAILS

The basic hodoscope circuit is shown in Figure 19. This circuit, which is due to Regener, uses only one electron tube per Geiger tube to turn off a neon bulb for about .1 second after a master pulse in all channels in which there was no coincident pulse from the Geiger tube. If there were a pulse from the Geiger tube the neon bulb would just stay lighted. The camera shutter is opened after the master pulse for about .05 second so that a picture is taken in which only those neon bulbs associated with discharged Geiger tubes are lighted. This mode of operation is free from the difficulties which occasionally arise from long delays between the application of voltage to a neon bulb and ignition. Figure 19 also shows the hodoscope driver circuit which supplies the master pulse to the hodoscope channels. The width of the master pulse must be less than the width of the pulses from the Geiger tubes in order for the hodoscope to function properly. The camera shutter was a "homemade" device in which a thin vane was moved in front of the lens by a "Husky" Rotary Driving Mechanism.* The coil of this device was pulsed by the shutter drive circuit shown in Figure 20. The 16 mm camera film was continuously advanced at the rate of 100 ft per week and the hodoscope pictures were correlated with the air shower experiment record with the aid of a clock which was photographed along with the neon bulbs.

The Detector II circuit, which uses transistors and was operated with a battery power supply, is shown in Figure 21.

All of the Geiger tubes were made from 1-inch o.d. brass tubing with .5 mm walls. The filling gas was a Petroleum Ether -- Argon mixture which not only gives very long plateaux (about 300 v) but also has the advantage that the tubes work well at even the lowest temperatures of the winter season.

Several procedures were used to ensure that the hodoscope circuits were operating correctly at all times. The pulse from the Geiger tube could be observed with an oscilloscope

---

* Type 76 Basic Rotary Driving Mechanism with 28V. coil. Price Electric Corporation, 5560 Church Street, Frederick, Md.

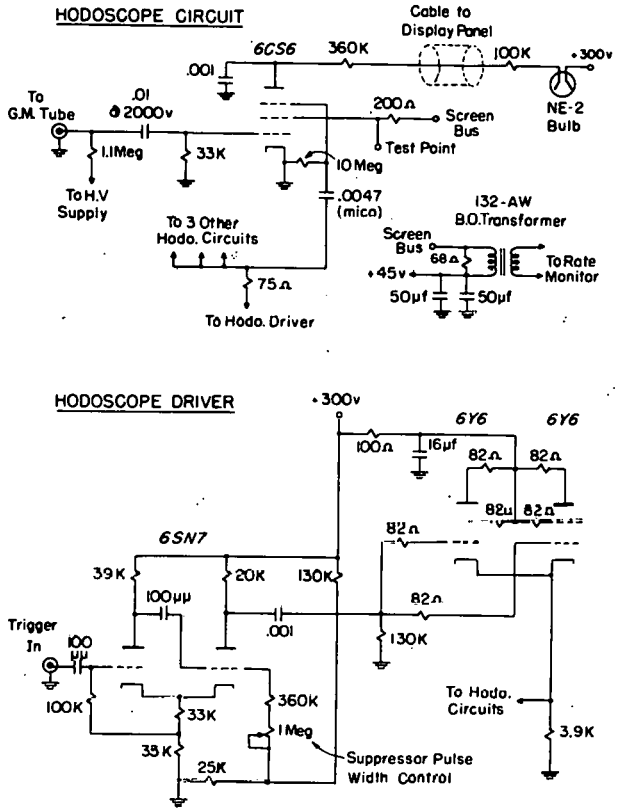

Figure 19

at the test point for each hodoscope channel. (See Figure 19.) Each Geiger tube was checked in this way at least once a week.

The operation of the circuits was checked by making sure that all the neon bulbs went out when a master pulse was applied. The screen voltage and shutter open time were varied while this was being done in order to make sure that all the circuits would operate even under adverse conditions.

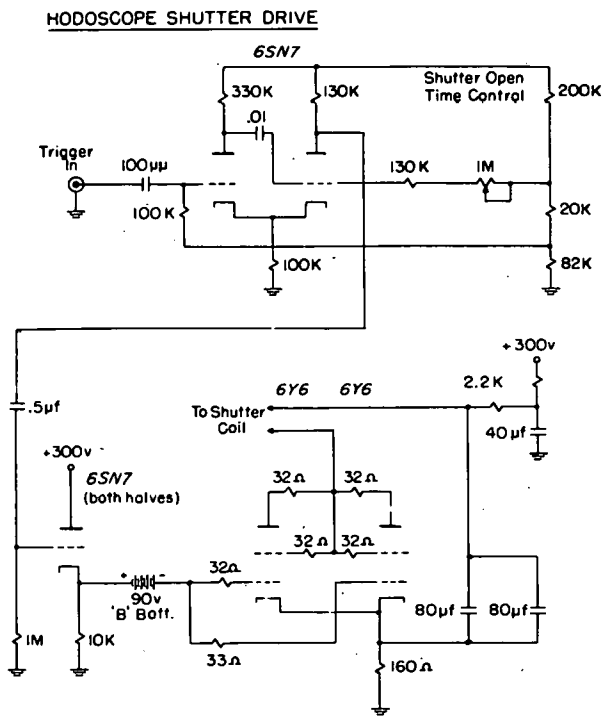

Figure 20

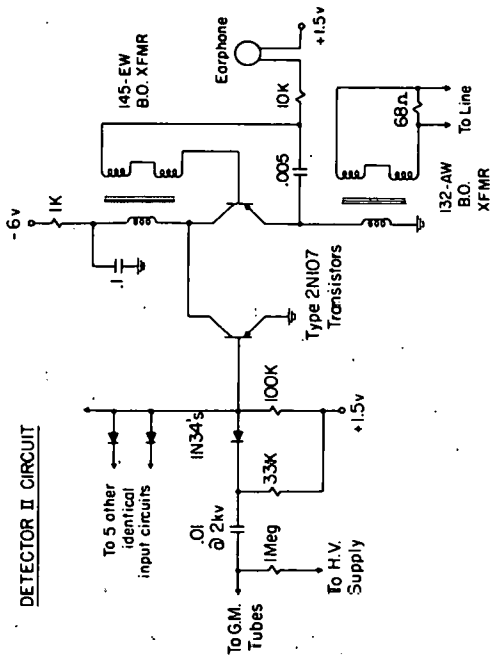

Figure 21

APPENDIX II

GEOMETRIC PROBLEMS

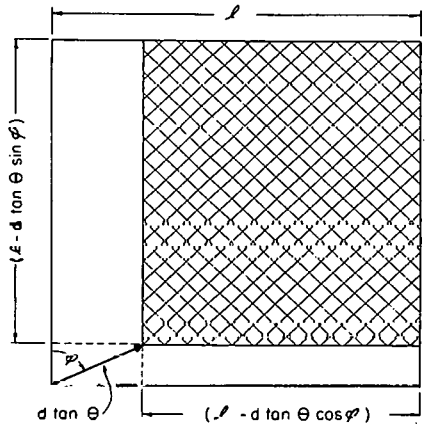

Figure 22

Figure 22 is a diagram showing a top view of the hodoscope detector. If mesons come in with zenith angle θ and azimuth ϕ, it is apparent that only those that go through the shaded area in the top tray will traverse both trays of the hodoscope. From the dimensions indicated in Figure 22 we find that the projection of this area in a plane normal to the direction of the mesons is:

$$A(\theta,\phi) = \cos\theta\ (\ell - d\tan\theta\cos\phi)\ (\ell - d\tan\theta\sin\phi)$$

$$= A_o \cos\theta \left\{ 1 - \frac{d}{\ell}\tan\theta\,(\cos\phi + \sin\phi) + \frac{d^2}{\ell^2}\tan^2\theta\ \cos\theta\sin\phi \right\}$$

where $A_o = \ell^2$ is the area of the trays. We are interested in the area averaged over all values of ϕ. Since $\frac{1}{2\pi}\int_o^{2\pi}(\cos\phi\,\sin\phi)d\phi = \frac{4}{\pi}$ and since the factor $\frac{d^2}{\ell^2}\tan^2\theta$ is very small for all values of θ of interest to us we have:

$$A(\theta) = A_o\ \cos\theta \left\{ 1 - \frac{4}{\pi}\ \frac{d}{\ell}\ \tan\theta \right\}$$

From this expression it is clear that the density for showers coming in at all azimuths is given by:

$$\rho = \frac{N_\mu}{A_0 \cos\theta \left\{1 - \frac{4}{\pi}\frac{d}{\ell}\tan\theta\right\}}$$

which is identical to Equation II (2).

From Figure 22 it is also apparent that the value of M (see Equation I(1)) is given, in terms of θ and ϕ, by:

$$M = d \tan\theta \sin\phi$$

This expression was used to relate the observed value of M to the angles θ and ϕ which were given by the air shower experiment.

From the geometry of the hodoscope and from the theory of statistical errors it is a simple matter to show that the fractional error in the absorption between the trays is given by:

$$\frac{\Delta f}{f} = \frac{1}{f\sqrt{N_T}} \sqrt{1 + \frac{8}{3\pi}\frac{d}{\ell}\tan\theta}$$

where f is the fractional absorption, N_T is the total number of mesons going through both trays, and $\Delta f/f$ is the fractional error in f.

APPENDIX III

TABULATION OF DATA

Most of the column headings have been discussed in the text or are identified in Table III. The data in each line of the tables refer to all the showers which fell within a certain radial interval. If there were less than three showers in a group, the data was not tabulated. The column headed S (for sample) presents the number of showers from a completely analyzed sample of 242 showers which fell in the group. The column headed C (for culls) presents the number of showers from a set of 663 showers which had an indication on the hodoscope record and fell in the group. The last column presents the total number of showers in the group, including those of the 663 that were not analyzed. This total number was computed from:

$$N_T = N_S + \frac{663}{242} S - C.$$

The asterisks* in the last column indicate the number of showers in the group whose hodoscope records were too complicated to be interpreted.

$10^6 - 3 \times 10^7$ $\theta < 25^o$

r	ρ/N	N_S	N_u	N_A	N_B	$\bar{\theta}$	$\bar{N_C}$	S	C	L
										**
13		14	61	302	212	14	3.0			**
25	.85 ± .1	22	67	179	127	15	3.4			**
42	.77 ± .05	77	205	338	290	15	3.0			
64	.42 ± .03	125	204	318	288	14	3.3			
106	.27 ± .02	238	315	482	428	13	4.2	2	3	241
170	.125± .008	266	241	386	353	15	6.3	4	15	266
268	.044± .004	292	102	162	144	14	4.2	79	34	474
376	.016- .004	133	20	38	35	14	4.1	51	25	249

10^6 - 3 x 10^7 $25 < \theta < 33^o$

r	ρ/N	N_s	N_u	N_A	N_B	$\bar{\theta}$	$\overline{N_e}$	S	C	L
14		7	8	80	84	30	1.5			**
24	1.38 ±.27	10	26	90	81	29	2.5			**
41	.68 ±.15	15	22	51	45	29	2.3			
65	.38 ±.05	42	61	103	99	28	4.0			
105	.23 ±.03	66	64	122	107	30	4.5			
166	.16 ±.02	92	73	166	122	27	5.1	2	3	94
266	.13 ±.02	91	40	79	73	29	3.7	18	20	120
380	.11 ±.03	35	12	18	19	27	3.3	10	7	55

10^6 - 3 x 10^7 $33^o < \theta < 40^o$

19		3	14	31	20	34	1.3			
27	1.25 ±.4	4	8	24	21	37	1.7			
40	.95 ±.3	7	12	21	20	36	1.9			
64	.46 ±.1	21	23	63	54	35	3.0			
102	.37 ±.06	36	41	104	80	36	3.9			
165	.22 ±.04	36	33	56	60	35	5.1			
266	.18 ±.04	38	21	39	30	36	3.7	8	9	51
378	.007±.04	17	4	10	13	36	3.8	5	2	29

$10^6 - 3 \times 10^7$ $40^\circ < \theta < 45^\circ$

r	ρ/N	N_s	N_u	N_A	N_B	$\overline{\theta}$	$\overline{N_e}$	S	C	L
		--								
		--								
38	2.3 $\pm$.6	5	14	24	24	42	1.8			
64	.80$\pm$.22	9	13	26	31	42	2.7			
99	.28$\pm$.09	11	11	30	24	42	4.1	1	1	13
174	.28$\pm$.07	15	7	32	28	42	3.8	2	2	18
250	.34$\pm$.1	13	12	20	29	42	4.0	1	3	13

$N_e = 1 - 3 \times 10^5$ $\theta < 25^\circ$

		--								
23	3.6 $\pm$ 3	2	2	2	2	20	2.6			
37	.9 $\pm$.9	4	1	1	1	19	2.5			
59	1.3 $\pm$.7	10	3	3	5	14	2.3			

$N_e = 3 - 10 \times 10^5$ $\theta < 25^o$

r	ρ /N	N_s	N_u	N_A	N_B	$\bar{\theta}$	$\overline{N_e}$	S	C	L
13	---	7	11	38	38	11	5.1			*
26	.9 ±.3	15	11	60	14	16	7.0			
40	.9 ±.2	35	21	41	43	15	5.8			*
61	.21 ±.05	40	7	10	18	14	6.1			
97	.16 ±.09	22	3	6	6	14	7.5			
143	---	3	0	0	0	15	9.6			
287	.045±.045	23	1	5	2	17	8.5	8	2	43
364	.084±.084	12	1	5	1	16	8.7	7	2	29

$1 - 3 \times 10^6$ $\theta < 25^o$

12		7	44	132	72	17	1.4			*
26	.86 ±.16	16	30	66	41	15	1.9			
42	.95 ±.1	57	124	192	178	16	2.0			
65	.46 ±.05	82	82	133	118	13	1.9			
104	.29 ±.03	125	78	116	105	14	1.9			
168	.17 ±.03	74	29	41	41	14	2.0	1	2	75
275	.66 ±.1	138	35	48	47	15	1.9	45	19	242
369	.28 ±.1	75	9	15	15	14	1.7	37	12	164

$3 - 10 \times 10^6$ $\theta < 25^\circ$

r	ρ/N	N_s	N_u	N_A	N_B	$\bar{\theta}$	$\bar{N}_e$	S	C	L
										**
14	---	7	17	170	130	10	3.5			**
24	1.4 ±.2	5	37	71	53	17	5.9			
44	.62 ±.08	17	60	117	85	15	5.0			
65	.44 ±.05	38	90	136	130	16	4.7			
108	.3 ±.025	95	171	255	224	14	5.0	2	1	100
169	.145±.014	149	137	215	205	15	5.6	2	10	149
265	.035±.005	122	41	67	55	14	5.3	31	11	196
390	.01 ±.003	48	9	21	14	15	5.7	13	11	72

$1 - 3 \times 10^7$ $\theta < 25^\circ$

--										
--										
43	.56 ±.14	3	21	28	27	14	1.1			
58	.37 ±.1	5	32	48	40	18	1.5			
109	.20 ±.03	18	66	110	99	16	1.6			
174	.095±.01	43	75	130	107	16	1.6	1	3	43
252	.05 ±.01	32	26	47	42	13	1.4	3	5	35
364	.01 ±.007	10	2	2	6	16	1.7	1	2	11

$3 - 10 \times 10^7$ $\theta < 25^o$

r	ρ/N	N_s	N_u	N_A	N_B	$\bar{\theta}$	$\overline{N_e}$	S	C	L
60	.29 ±.06	2	23	35	34	15	3.5			
92	.056±.02	3	9	46	33	17	4.7			*
167	.067±.01	10	44	79	61	12	5.7			
260	.037±.01	7	14	32	21	16	4.7			

$3 - 10 \times 10^5$ $25 < \theta < 33^o$

25	1.12 ±.55	5	4	7	7	30	7.5			
39	.81 ±.37	9	5	6	9	28	7.2			
66	.75 ±.36	11	5	5	7	29	6.4			
98	.40 ±.18	14	4	5	7	29	7.5			
—	—	—	–	–	–	—	—			
288	.16 ±.16	9	1	2	2	28	6.9	1	2	10
380	.27 ±.27	4	1	3	1	29	8.1	1	2	5

$1 - 3 \times 10^6$ $25 < \theta < 33^\circ$

r	ρ/N	N_s	N_u	N_A	N_B	$\bar{\theta}$	$\bar{N}_e$	S	C	L
14	---	7	8	80	84	30	1.5			**
26	2.0 $\pm$.43	7	21	31	38	30	1.6			
41	.71 $\pm$.2	12	12	26	25	29	1.5			
63	.67 $\pm$.11	29	35	61	50	29	1.9			
104	.23 $\pm$.06	36	15	32	26	28	1.9			
163	.13 $\pm$.04	33	10	16	21	28	2.0			
272	.081$\pm$.03	47	11	17	16	28	2.0	13	10	72
380	.053$\pm$.03	18	3	4	6	27	2.0	7	6	31

$3 - 10 \times 10^6$ $25 - 33^\circ$

23	.53 $\pm$.2	3	7	58	43	28	4.7			**
47	.75 $\pm$.3	3	10	18	26	31	4.7			
69	.29 $\pm$.09	8	9	14	21	28	4.1			
106	.25 $\pm$.05	23	26	48	49	28	4.8			
167	.20 $\pm$.03	48	48	75	74	29	5.3	1	3	48
264	.067$\pm$.03	33	11	27	25	28	4.7	4	8	37
379	.093$\pm$.03	15	9	13	13	28	4.7	3	2	22

$1 - 3 \times 10^7$ $25 - 33^\circ$

r	ρ/N	N_s	N_u	N_A	N_B	$\bar{\theta}$	$\overline{N_e}$	S	C	L
69	.23 ±.06	5	17	28	28	26	1.6			
112	.21 ±.04	7	23	82	68	28	1.7			*
159	.11 ±.03	11	15	24	27	27	1.3	1	0	11
242	.099±.025	11	18	33	32	28	1.6	1	2	12*

$3 - 10 \times 10^5$ $33 - 40^\circ$

44	.515±.3	11	3	10	17	35	6.4			
61	1.17 ±.6	6	4	7	6	36	6.9			
103	.48 ±.34	6	2	2	2	36	8.5			
--	---	--	-	--	--	--	---			
249	.38 ±.38	5	1	1	1	35	6.4	2	1	10
359	---	6	0	1	0	36	6.4	3	1	14

$1 - 3 \times 10^6$ $33 - 40^\circ$

r	ρ /N	N_s	N_u	N_A	N_B	$\bar{\theta}$	$\overline{N_e}$	S	C	L
19	---	3	14	31	20	34	1.3			
27	1.43 $\pm$.5	4	8	24	21	37	1.7			
39	.95 $\pm$.34	6	8	15	22	36	1.7			
63	.5 $\pm$.14	15	13	43	36	35	2.1			
104	.39 $\pm$.1	23	14	34	29	36	1.9			
167	.27 $\pm$.11	15	6	15	10	36	1.8	0	2	15
289	.05 $\pm$.04	18	2	3	7	36	1.8	5	4	27
384	---	6	0	0	0	36	1.8	4	0	18

$3 - 10 \times 10^6$ $33 - 40^\circ$

67	.37 $\pm$.1	6	10	20	18	36	5.4			
93	.31 $\pm$.1	9	10	28	21	35	4.3			
161	.21 $\pm$.06	15	13	23	23	36	5.1			
250	.15 $\pm$.04	17	14	25	17	35	5.5	3	6	20
376	.10 $\pm$.05	8	4	7	13	36	5.4	1	2	9

$1 - 3 \times 10^7$ $33 - 40^\circ$

r	ρ /N	N_s	N_u	N_A	N_B	$\bar{\theta}$	$\bar{N}_e$	S	C	L
108	.36 ±.09	3	17	32	24	34	1.9			
168	.22 ±.06	6	14	18	27	34	1.3			
229	.15 ±.07	3	5	10	6	36	1.3			
376	---	3	0	2	0	36	1.3			

$1 - 3 \times 10^6$ $40 < \theta < 45^\circ$

38	2.3 ±.6	5	14	24	24	42	1.8			
67	.94 ±.4	6	6	10	12	42	1.6			
91	.41 ±.25	5	3	5	7	42	2.2			
174	.19 ±.13	7	2	4	5	43	1.6	1	0	10
256	.19 ±.13	6	2	4	4	41	2.0	1	1	8
		24	24	47	45	42	1.9	2	1	

$3 - 10 \times 10^6$ $40 < \theta < 45^\circ$

57	.7 ±.3	3	7	16	19	41	5.0			
106	.23 ±.09	6	8	25	17	42	5.7	1	0	9
175	.13 ±.06	6	4	11	9	41	5.9	1	1	8
250	.21 ±.1	6	5	8	13	42	4.7	0	1	6

Data from Detector II

N_N \ θ_N	1	2	3	4	5
2	1 (17)	0 (2)	1 (5)	(3)	(6)
3	1 (91)	1 (23)	1 (11)	0 (4)	1 (4)
4	7 (54)	1 (9)	1 (0)	(2)	(2)
5	1 (5)	(3)			
7	(1)	1			1

θ_N and N_N are defined in Table IV.

Numbers with no parentheses are the number of showers in a sample of 1600 which triggered Detector II and had the indicated combination of θ_N and N_N.

Numbers in parentheses are the number of showers in the sample of 242 showers which had each combination of θ_N and N_N. The total number of showers in each box was obtained by multiplying the number in parenthesis by 1600/242.

BIBLIOGRAPHY

(BD 47) Broadbent, D. and L. Jannosy, Proc. Roy. Soc., A191, 517 (1947)

(BWW 49a) Brown, W. W., A. S. McKay and E. D. Palmatier, Phys. Rev., 76, 506 (1949)

(BWW 49b) Brown, W. W., and A. S. McKay, Phys. Rev., 76, 1034 (1949)

(CB 48) Chowdhuri, B., Proc. Phys. Soc., A63, 165 (1948)

(CG 49) Cocconi, G., Phys. Rev., 75, 1058 (1949)

(CG 49a) Cocconi, G., V. C. Tongiorgi and K. Greisen, Phys. Rev., 75, 1063 (1949)

(CG 49b) Cocconi, G., V. C. Tongiorgi and K. Greisen, Phys. Rev., 76, 1020 (1949)

(CGW 57) Clark G. W., J. Earl, W. Kraushaar, J. Linsley, B. Rossi, and F. Scherb. To be published soon in Nature.

(CU 50) Camerini, U., P. H. Fowler, W. O. Lock, H. Muirhead, Phil. Mag., 41, 413 (1950)

(DNA 56) Dobrotin, N. A., G. T. Zatsepin, S. I. Nikolski and G. B. Khristiansen, Nuovo Cimento Supplemento 3, 635 (1956)

(ELC 52) Eidus, L. C., M. I. Adamovitch, I. A. Ivanovskaya, V. S. Nikolaev and M. S. Tulyankina, JETP, 22, 440 (1952)

(FE 50) Fermi, E., Prog. Theor. Phys., 5, 570 (1950)

(FG 53) Fujioka, G., International Conf. Theo. Phys. (Japan)

(GK 50) Greisen, K., W. D. Walker and S. P. Walker, Phys. Rev., 80, 535 (1950)

(GK 56) Greisen, K., Progress in Cosmic Ray Physics, Vol. II (Amsterdam: North Holland Publishing Co.) Chap. I.

(KML 54) Kasnitz, H. L., and K. Sitte, Phys. Rev., 94, 977 (1954)

(OS 57) Olbert, S., and R. Stora. Private communication from S. Olbert.

(PNA 57) Porter, N. A., and A. C. Sherwood, Harwell Report, A. E. R. E. NP/R2110

(SG 49) Salvini, G., and G. Tagliaferri, Nuovo Cim. 6, 108 (1949)

(SRP 56) Shutt, R. P., Proceedings of the Sixth Annual Rochester Conference, 1956, Interscience Publishers

(TJE 48) Treat, J. E., and K. Greisen, Phys. Rev., 74 414

(ZGT 53) Zatsepin, G. T., I. L. Rosental, L. I. Saritcheva, G. B. Khristiansen, and L. C. Eidus, Isv. Akad. Nank, SSSR, Ser. Fiz., 17, 39 (1953)

ACKNOWLEDGEMENTS

The present measurements were possible only through the co-operation and assistance of many people affiliated with the Laboratory for Nuclear Science and the Harvard College Observatory.

In particular, the author is grateful for the assistance and guidance of Professor William L. Kraushaar throughout the work.

The author would like to thank Professors Stanislaw Olbert and Satio Hayakawa for many profitable discussions concerning the interpretation of the results.

Charles Fernald, Charles Forte, Edward Mangan, and Robert Mudge constructed all of the equipment, including the Geiger tubes. Their help in this and in setting up the experiment is gratefully acknowledged.

The personnel of the Laboratory Stock Room under the supervision of Mr. V. Scrima and Mr. S. Tardivo worked long hours moving the lead shielding.

Mrs. June Massy and Mrs. Barbara Corcoran punched the data onto IBM cards.

The assistance of Mr. Frank Scherb in expediting the processing of showers on the Whirlwind computer was invaluable.

Mrs. Prabha Madan and Mrs. Micheline Quequin prepared the showers for the Whirlwind analysis.

The co-operation of Mr. Russell Anderson of the Harvard Observatory Staff greatly simplified the work of setting up the experiment.

To all of the above and to any he has omitted, the author expresses his thanks and gratitude.

BIOGRAPHICAL NOTE

The author was [redacted] He attended the public schools in Omaha and entered the Massachusetts Institute of Technology in 1949. He received the degree of Bachelor of Science in June, 1953 and enrolled in the Graduate School of the Massachusetts Institute of Technology during the same year. During the period November 1953 to June 1954 he was a Teaching Assistant at MIT and in June 1954 was appointed Research Assistant in the Laboratory of Nuclear Science.

Publications:

(1) A Simple Pump for Circulating Pure Gas,

James A. Earl, Review of Scientific Instruments, Vol 25 p 397 (1954)

(2) An Experiment on Air Showers Produced by High Energy Cosmic Rays,

G. Clark, J. Earl, W. Kraushaar, J. Linsley, B. Rossi, and F. Scherb.

To be published in Nature.